Analysis of the physicochemical detectability and impacts of offshore CO_2 leakage through multi-scale modelling of in-situ experimental data using the PLUME model

Marius Dewar[a,b], Umer Saleem[b], Anita Flohr[c], Allison Schaap[c], James Strong[c], Jianghui Li[d], Ben Roche[c], Jonathan M. Bull[c], Baixin Chen[b], Jerry Blackford[a]

[a]*Plymouth Marine Laboratory (PML), Prospect Place, The Hoe, Plymouth PL1 3DH, UK*
[b]*Institute of Mechanical, Process and Energy Engineering, Heriot-Watt University, Edinburgh, UK*
[c]*Ocean and Earth Science, University of Southampton, National Oceanography Centre Southampton, Southampton SO14 3ZH, UK*
[d] *Institute of Sound and Vibration Research, University of Southampton, Southampton, UK*

Abstract

Carbon storage is required to keep rising global temperatures below 2 °C, meanwhile, storage reservoirs monitoring is required for assurance of early detection of potential leakages. Projects such as QICS and STEMM-CCS have used small in-situ experiments to develop detection techniques, tools, and strategies. Given the expense of experiments it is crucial to develop accurate simulation models that replicate observed behaviours and can be extrapolated to many different scenarios. However, anomalies occur between modelled and experimental data, and a key question has been how can the models be improved?

This has been approached through the development of a complex modelling system to include the effects of coastal hydrodynamics on very localised experiments, with a new multi-phase leakage model – PLUME, integrated into a high-resolution hydrodynamic model, and linked to a carbonate system for CO_2 analysis. The resolution of the nested domains range from 2.5 km at the boundaries to approximately 0.5 - 1.0 m at the release sites.

The efficacy of the PLUME model is demonstrated with application to the STEMM-CCS and QICS experimental sites in 120 and 9-12 m water depths respectively. Results show that the newly developed model can predict observed pCO_2 and pH changes within acceptable errors. Local effects are shown to be affected greatly by both the resolution and the water currents, with momentary spikes in pCO_2 and reductions in pH caused by tidal oscillation. The spatial impacts of the releases are shown to move with the tide, covering a far greater area over a tidal cycle.

Keywords: Carbon Capture and Storage, CCS, FVCOM, leakage, monitoring, marine, climate change, bubbles, multi-phase, CO_2

1. Introduction

Carbon Capture and Storage (CCS) is a necessary technique to mitigate the threat to the global climate from fossil fuel and other industrial sources of anthropogenic carbon dioxide (CO_2) emissions [1], along with the economic need to continue emissions for the short to medium term [2]. The Intergovernmental Panel on Climate Change (IPCC) reports [1], [3] indicate implementations of CCS at industrial scales could contribute to the reduction of CO_2 by the 80 - 95% by 2050, which is required to keep rising average global temperatures below 2 °C [1], [3]. CCS involves capturing CO_2 from point source emitters, compressing and burying the gas in geological formations. Utilising depleted oil and gas reservoirs or saline aquifers [3] deep below the seafloor has been proposed, developed and actively pursued since 1996, in part due to carbon taxes [4], [5].

With the need to transport CO_2 to potential offshore storage sites, a large proportion will lie in shelf seas near coastal communities. With energy generation and aquaculture amongst others, there is an increasing demand and activity within shelf seas, with a complex ecosystem (which has been shown to modulate the impacts of climate change through CO_2 uptake) that needs to be maintained [6], [7]. The practical adoption of CCS depends on the ability to demonstrate storage integrity in the context of both regulation [8] and public perception [9], with the need for a trusted monitoring strategy. A large concern in the past has been storage integrity and the likelihood of

leakage [10], [11], with the corresponding environmental impacts and the need for both storage monitoring strategies and leakage quantification [12]. Whilst now accepting that properly engineered storage is not expected to leak, regulatory agencies require assessments of the risk, with the potential impact to be both understood and quantified should CO_2 be released into the water column [13], [14].

Any acute impacts on marine biology would occur within the near field [15], which covers a scale of the seawater from meters up to kilometres. Full scale experiments, with large releases are potentially economic and environmentally expensive. Therefore small scale field and laboratory experiments are required [16], such as the Quantifying and Monitoring Potential Ecosystem Impacts of Geological Carbon Storage (QICS) project [13], Measurement, Monitoring and Verification of CO_2 Storage (MMV) and the Strategies for Environmental Monitoring of Marine Carbon Capture and Storage (STEMM-CCS) project experiments [17], with the development of numerical models to further understand the mechanisms of leakage from the seabed into the turbulent seawater, which can be relatively cheaply extrapolated to larger scale situations. This provides extensive data, filling the gaps and uncertainties left from small scale experiments alone whilst minimising economic and environmental cost [14], [18]–[29].

In low depth releases (< ~500 m) highly buoyant CO_2 gas bubbles rise as a plume into the water column, dissolving rapidly as the natural waters are undersaturated in CO_2 [27], [30]. This dissolved solution, results in an increase of Dissolved Inorganic Carbon (DIC) [31], and partial pressure of CO_2 (pCO_2). The solution also dissociates into carbonate, bicarbonate and hydrogen ions, with the increases in hydrogen ions reducing the pH of the seawater. CO_2 solution is slightly denser than the background [32], [33], sinking towards the seabed [25]–[27], and subsequently dispersed, driven by local hydrodynamics, surface winds, tidal mixing, turbulent diffusion, and residual circulation. In terms of the spatial extent of a release, depending on the release rate, it has been shown to only impact a very limited region of up to the order of a hundred meters immediately adjacent to the source, [14], [19], [26], [27], [34].

Existing models have several shortcomings beyond the lack of experimental data required to develop precise modelling systems. There is a shortfall in the number of multi-phase numerical models (models that can simulate more than one fluid) designed to predict leakages from low depth, dissolving, bubbly flow for CO_2 leakage scenarios [25]–[27]. Further to this, investigating leakage timeframes from days to weeks and beyond requires analysis in multiple scales [14], investigating the local impacts [14], [25]–[27] in the order of meters and the regional impacts [35] based on changes in currents and tide in the order of tens of kilometres. Except for the modelling system by Mori, Kano, Sato et al. [35], [36], there are a lack of multi-phase, multi-scale modelling systems allowing data transfer between each scale. Even so, the rectilinear mesh used therein can be computationally inefficient if applied over larger coastal areas. This suggests the need for development of a multi-scale, unstructured mesh model [37] for good simulations of turbulent flows around the coastline capable of calculating multi-phase hydrodynamics across the mesh.

In this study, a 3D physicochemical modelling system is developed for CO_2 leakage analysis in coastal waters, built on the unstructured-grid Finite-Volume Community Ocean Model (FVCOM) [37] to provide the local and regional hydrodynamics. The Predicting Leakage Using Multi-phase Equations (PLUME) model is developed and integrated as a two-way plume modelling system allowing investigation of localised physicochemical impacts utilising the carbonate system from European Regional Seas Ecosystem Model (ERSEM) [38] to analyse the ecosystem impacts.

The modelling system and domain are set on the tidally dominated north-west European continental shelf, utilising the Scottish shelf model mesh and boundary forcing system [39], providing inputs to internally nested domains for the specific sites for high resolution (500 m to 50 cm) analysis. The high-resolution domain allows localised physical and chemical analysis for both the coastal QICS CO_2 release experiment [13] in a semi-enclosed bay off the West coast of Scotland, and the off-shore STEMM-CCS CO_2 release experiment in the vicinity of the Goldeneye potential storage complex in the Northern North Sea.

From the QICS experiment, the first of its kind, large anomalies were found to occur between the experimental readings and the limited numerical models [25]. With the assistance of the new numerical modelling system, this study aims to resolve these anomalies in detectability and environmental impact findings and validate findings from both controlled sub-seabed release experiments of CO_2 (QICS and STEMM-CCS).

Table 1. The Experiment Characteristics

	QICS	STEMM-CCS
Water depth (m)	9-12	~ 120
Injection depth below the seafloor (m)	15	3
Injection rates (kg/day)	0 - 208	0 – 143
Sediment type	sandy	Clay

2. In-situ Experiments

This section outlines the background to this study, with experimental data and findings. The two experiments have similarities and significant differences as described in Table 1. As the QICS experiment was located in a semi-enclosed bay, the horizontal tidal currents were quite strong, up to 40.5 cm/s [40], and a water depth of ~10 m with a fully mixed water column. This compares with residual currents of up to 25 cm/s in the STEMM-CCS experiment [41] near to the Goldeneye complex at ~100 m depth, giving contrasting hydrodynamics and a stratified water column.

Both releases observe bubbly flow throughout the experiment, where the bubble formation is controlled by the structure of the seabed sediments and the fluid interactions as described in Dewar et al. [25]. Higher rates with flow from the seabed under pressure, would require jet dynamics affecting bubble sizes and water hydrodynamics.

2.1. The QICS Experiment

QICS was a project with the aim of improving the understanding of potential impacts that a leakage from carbon dioxide geological storage could have on the ecosystem, and to investigate a variety of techniques and methods that may be suitable for monitoring leakage. The experiment involved drilling a narrow borehole from land, terminating in unconsolidated sediments 10 m below the sea floor, with 9–12 m head of seawater in a semi-enclosed bay as shown in Figure 1a. The release was carried out in May – June 2012, continuing for 37 days with a cumulative release of 4.2 tonnes of CO_2 [13]. The data required to model the release experiment, other than the site-specific data (location, depth, salinity, temperature, currents), are the release rates to the seawater, bubble sizes, and pockmark distribution map. The bubble size distribution and pockmark positions are provided by Sellami et al. [28] as shown in Figure 2a and Figure 2b respectively. The size distribution was recorded from a small sample of the experiment as discussed by Sellami et al. [28]. However, due to the low flow rates from the seabed 15 meters above the injector, the gas lost its initial injection pressure and only rose through buoyancy. It is therefore possible to predict the size from the momentum, buoyancy and surface tension as described in Dewar et al [25] without any impact from the flow rate. Changes in pockmarks would however cause different sized bubbles to appear. The release rate to the water column has been taken from Bergès et al. [42] which showed the release rate in the final stages of experiment. The pattern that varies with the tide [13] has been extrapolated to the start of the experiment using the same injection rate / bubble release rate ratio as shown in Figure 2c. Background values for Total Alkalinity (TA) and DIC were measured as 2307 μmol/kg and 2128 μmol/kg respectively [43].

Anomalies were found to occur between experimental readings [13], [40], [44]–[47] and the numerical models [25], [35], [48]. The models under predicted physicochemical changes when simulating the physically measured seepage rate, based only on the observed gas flow rate (~15% of the injection rate [13]), providing maximum levels of pCO_2 of 443 – 530 μatm [25], [35]. This is compared to the experimental measured values of an average of 390 - 500 μatm, 30 cm above the seabed, but at times increasing up to 1200 - 1250 μatm, with occasional peak values of 1500 - 1600 μatm from observations 3 cm above the seabed [13], [40], [44], [45], showing the large differences over a very small distance. These findings therefore led to some conclusions that the seepage rates for CO_2 (gas bubbles and dissolved solution) from the seabed are still largely unknown, with uncertainties of potential CO_2 dissolving in the sediments prior to seepage [25], [35], [48]. This provides a build-up of DIC being released with the bubbles when the seepage rate increases at low tide, and small bubbles that couldn't be measured dissolving quickly in the water column [25], [35].

In this paper another mechanism is investigated; the seepage rate measurements are reasonable, but higher model resolution is required to be able to predict the high peaks, with the tidal cycle also having a large effect on the plume dynamics. This mechanism has been discussed [17], [48] but has yet to be demonstrated in practice.

2.2. The STEMM-CCS Experiment

The STEMM-CCS experiment, a controlled CO_2 release in the central North Sea near the Goldeneye platform, dominated by north-south tidal currents, aimed to expand upon knowledge gained from the QICS experiment amongst others [41] as shown in Figure 1b. This experiment was designed to imitate an unintended release of CO_2 from a geological CO_2 storage site to the seabed. The main objective was to advance the fundamental understanding of the marine environment impacts above a CO_2 storage site, also through detecting, characterising and quantifying gaseous and dissolved CO_2, provide cost-effective environmental monitoring and leakage quantification techniques [41]. The experiment involved inserting a pipe into unconsolidated sediments 3 m below the seabed, with ~120 m head of seawater in open waters. The release was carried out in May 2019, continuing for just over 12 days.

As with the QICS experiment, the release rates, bubble sizes, and pockmark distribution map are required for modelling. These parameters were recorded through optical, acoustic and gas collection techniques through use of remotely operated vehicles (ROV), autonomous underwater vehicles (AUV), optical landers and hydrophone arrays [41].

Bubble sizes were predicted by passive acoustics and gas bubble imaging, giving the bubble size distribution shown in Figure 3a [49], and a map of the bubble streams was collated as shown in Figure 3b. The gas flow rate into the sediments was initially set to 6 kg/d, and then sequentially increased over the duration of the experiment to a maximum of 143 kg/d with a cumulative release of 675 kg of CO_2 [41] as shown in Figure 3c. As with the QICs experiment, the size distribution is recorded from a small sample of the experiment as discussed by Li et al. [49]. However, due to the low flow rates from the seabed, the flow rate does not impact the bubble size [25]. Changes in pockmarks would however cause different size bubbles to appear.

Estimates of the release rate to the seawater derived using the gas bubble sampler's inverted funnel (seep flow rate measurements) showed that the total seepage rates increased from a minimum of ~1.3 kg CO_2 d^{-1} (22%) at the lowest injection rate to a maximum of ~70 kg CO_2 d^{-1} (48%) at the highest injection rate [50], also shown in Figure 3c, with the rest retained or ejected as a dissolved solution. This is to be compared with the data from eddy covariance techniques that predicted a best estimate of up to 66 ± 19% [51]. Similarly, measurements of benthic gradients of pH using lab-on-chip sensors yielded estimates of 42±17% [52].

No bubbles were found to be visible higher than 8m above the seabed [41] showing the fast dissolution rate. pH changes were recorded using lab-on-chip pH sensors, giving a reduction of up to 0.6 units as a peak at ~2.6 m downstream of the plume, with the typical reduction of ~0.3 units during the largest injection rate (143 kg/d) when the tide pushed the flow past the sensor [52]. Background values for TA were measured as 2310 µmol/kg, with the corresponding background DIC derived as 2140 µmol/kg [52].

3. Modelling System

This section outlines the principal aspects of the study, with the development and application of the hydrodynamic multi-scale and multi-phase modelling system. To investigate the fate and impacts of leakage into the local environment, model coupling and nesting are required. As shown in the experiments in Section 2, the CO_2 plume of bubbles manifests locally from centimetres to tens of meters. In order to investigate and predict the plume dynamics, including rise height, horizontal movements, rate of dissolution, and concentration distribution of the CO_2 solution, the Predicting Leakage Using Multi-phase Equations (PLUME) model is developed, with the ability to nest into various oceanic hydrodynamic and biogeochemical modelling systems.

Interactions of bubbles with seawater are affected greatly by small scale ocean dynamics, such as tides, currents, and turbulence, which, however, develop at scales from global, coastal, regional, down to the local environment. These cascading hydrodynamics are modelled by FVCOM [37], and biogeochemical changes to the water column, delineate the overall fate and impacts in the water column. These are obtained from offline linking of the plume and ocean hydrodynamic models to the carbonate system [20], [53] from ERSEM [54]. An interaction chart is provided in Figure 4 showing how the models (PLUME, FVCOM, and ERSEM) interact with each other within the modelling system, communicating through the physiochemical and biogeochemical variables.

3.1. PLUME

The PLUME model is developed (based on the governing equations from the individual bubble model by Chen et al. [30]), that not only resolves the bubble dynamics, but further provides plume dynamics, and provides source terms for changes in mass, momentum and dissolved solutions in the water column to the ocean hydrodynamic and biogeochemical models. The model is a Lagrangian based system, with a set of non-linear ordinary differential equations, which are numerically solved by using the fourth order Runge-Kutta method.

PLUME is a general model designed to simulate the interaction dynamics of gas bubbles, liquid droplets, solid particles, or a combination, with the surrounding fluids dependant on the field of study. In this model, the dynamics of parcels, or collections containing a set number of similar 'objects' whether they are bubbles, droplets, or particles (BDPs), are simulated. The number of BDPs in this parcel can be defined and set by the release rate and size distributions as the input. There are no limitations on the number of the BDPs in the parcel, but they require to have similarity in all physical, chemical and biological properties as defined with the given distribution.

For leaked or released CO_2 in seawater, PLUME interlinks with the hydrodynamic model to bring in the local fluid properties, including the seawater density, currents, temperature, salinity, along with background concentrations of dissolved solutions (such as CO_2). PLUME then outputs impacts from the BDPs on momentum and mass from the dissolved solution back to the hydrodynamic model as shown in Figure 4.

3.1.1. Governing equations

Consider a collection of objects or BDPs as a parcel, the BDPs in the parcel interact with the surrounding fluids in mass and momentum exchanges under a thermal equilibrium condition. The total exchange rates of mass and momentum of the BDPs with respect to time can be presented by conservations of mass and momentum (Newton's 2nd law) as,

$$\frac{dm_p}{dt} = N_o \dot{m}_o + m_o \dot{N}_o \qquad (1)$$

$$\frac{d(m_p u_{r,p})}{dt} = \sum_{j=1}^{n} F_j \qquad (2)$$

where N_o and $m_o$are the number of objects, and mass (kg) of each BDPs in the parcel, with m_p as the total mass of the parcel, u_r is the relative velocity vector of BDPs to that of the surrounding fluids (m/s) and F_j are forces acting on the parcel (N). The subscript p indicates the parcel, o the objects or BDPs, and j the forces acting on the BDP.

N_o is initially set for each parcel through the conservation of mass (Eq. 1), assuming a constant number of objects in the parcel (removing the second term). With a given mass release rate, timestep, density and BDP diameter/size/volume provided by a size distribution, the initial number of BDPs in each parcel can be predicted. Two mechanisms can change the total number of BDPs and the distribution in the parcel after release, the breaking up and collision. Details can be found from the previous studies [25], [55]. From the field measurements of QICS [28] and STEMM-CCS [48], it is confirmed that both the breaking up and coalescence were rarely observed from these CO_2 bubble plumes, and are shown to have a minor effect [25]. Therefore, the changes in total bubble number in the parcel are neglected in this study.

The mass exchange rate of the BDPs in the parcel can be calculated by the dissolution rate,

$$\dot{m}_o = -k_o A_o (C_s - C_b) \qquad (3)$$

where k_o(m/s) is the effective mass transfer coefficient, A_o (m^2) the total surface area of the BDP, C_s the solubility (kg/m^3) and C_b the background concentration in surrounding waters (kg/m^3). Combining Eq. (1) with Eq. (3) and resolving the geometry (considering each BDP as a sphere to define the equivalent diameter d_e), the dissolution rate of each BDP in each parcel can be predicted through the equivalent BDP diameter shrinking, at a rate of

$$\dot{\bar{d}}_{e_o} = -\frac{1}{\rho_o}\left(\frac{\bar{d}_{e_o}}{3}\dot{\rho}_o + 2\,k_o(C_s - C_b)\right) \qquad (4)$$

where ρ_o is density (kg/m^3) of the BDPs. The first bracketed term on the right-hand side of Eq. (4) gives the effect of compressibility of the BDP to changes in bubble size. The momentum exchange of BDPs in the parcel with surrounding fluids can be identified by the forces acting on each individual BDP from both drag and buoyancy. Adding these forces into equation (2) and resolving for a spherical object, gives the changes in relative velocity of the parcel $u_{r,p}$ (or the individual BDP with an equivalent size of d_e) as

$$\dot{u}_{r,p} = \gamma_\rho\left(\left(1-\gamma_\rho^{-1}\right)g - \frac{3u_{r,p}^2}{4d_e}c_d\right) - u_{r,p}\frac{\dot{m}_o}{m_o} \qquad (5)$$

where, c_d is the drag coefficient of each BDP in the surrounding fluids, g is gravity, $\gamma_\rho$is the density ratio of surrounding fluids to the BDP.

3.1.2. Communication with hydrodynamic and ecosystem models.

The PLUME model communicates through interacting with oceanic hydrodynamic and ecosystem models. As shown in Figure 4. PLUME extracts the 3D currents, pressure, temperature, salinity and density of seawater, along with background concentrations of dissolved solution from the oceanic hydrodynamic model, meanwhile providing the dissolved mass, the position of the BDP, and the drag force acting on the surrounding seawater as a momentum source. These exchange rates of mass and momentum to the seawater in the oceanic hydrodynamic model are predicted by PLUME by the following source terms,

$$S_{Mass} = \dot{m}_P\frac{\Delta t_P}{V_H\Delta t_H} \qquad (6)$$

$$S_{Mom} = \dot{u}_{r,p}\left(\frac{V_P}{V_H}\frac{\Delta t_P}{\Delta t_H}\right) \qquad (7)$$

where V_P and V_H are the volumes of the parcel and the hydrodynamic model's grid cell corresponds with the parcel position, Δt_P and Δt_H are the time steps of the PLUME model and the hydrodynamic model, respectively.

3.2. ERSEM

ERSEM is a comprehensive biogeochemical and ecological model [54] from which the carbonate system is extracted to predict changes in pH, pCO_2 etc. The carbonate system was first introduced to ERSEM by Blackford and Burkill [56] using the HALTAFALL speciation code from Ingri et al. [57]. The changes in pH and pCO_2 are calculated from the modelled aqueous CO_2, salinity and temperature values, along with background values of DIC, TA and total boron [20], [54]. The DIC can be predicted from the addition of the aqueous CO_2 to the background DIC measurements. Further details on the ERSEM carbonate system module can be found in Artioli et al. [38] and Butenschön et al. [54].

3.3. FVCOM

FVCOM is the base model in this system with which the other models interact. It is a unstructured-grid, coastal hydrodynamic circulation model [37], with the atmospheric weather forcing through the free surface. The primitive 3D equations of continuity, momentum, energy and tracers (salinity and CO_2 solution) are solved to simulate the multiscale dynamics of the hydrodynamic turbulent flows, which are coupled with the PLUME model (Section 3.1) and outputting to ERSEM (Section 3.2).

FVCOM has an increasing user base, utilised in a range of various research areas, and has been widely used for simulating hydrodynamics in coastal and shelf waters due to the bathymetry following mesh system and nesting capabilities for high resolution analysis. As a brief and very limited summary, modelling topics have included the stratification and mixing of temperature and salinity [58]–[62], marine renewables [63]–[65], ecosystem and marine habitats [66]–[72], and detection of dissolved CO_2 plumes release as single phase in coastal waters [18], [29].

For coupling, modifications have been made to the FVCOM code to allow the source terms to be added into the governing equations, through Eq. (6) and (7) above. Taking the FVCOM equations, the momentum source (S_{Mom}) is added on the right hand side of the vertical momentum equation: Eq. (2.2) in Chen et al. [37]. And the dissolved mass source (S_{Mass}) replaces the source term (C_o) in the Tracer-Tracking module equation: Eq. 12.1 in the FVCOM Manual [73]. Also, dissolution in seawater causes a change in seawater properties, not only a reduction in dissolution rate from saturation levels shown in Section 2.1, but also changes in seawater density. Therefore, the calculations for seawater density are extended in FVCOM to include the CO_2 concentration as given by Song et al. [32], [33].

3.4. Modelling System Setup and Process

To account for the tidal and coastal currents and to include high resolution around the experimental sites, a nested configuration is used within FVCOM. The large domain covers the North Sea and waters surrounding the UK. The Scottish Shelf Model is utilised [6] to set up the model domain and boundary forcing (shelf wide domain, version 2.01, [74]), as shown in Figure 5a, and to provide forcing data at the nested boundary of the high resolution model domain, shown in Figure 5b and Figure 5c. The nested domains have a resolution ranging from 2.5 km at the boundary to approximately 0.5 - 1.0 m at the CO_2 release sites.

The bathymetry is set by data from the European Marine Observation and Data Network (EMODnet) and the North-West Shelf Operational Oceanographic System (NOOS), the latter, for the North Sea east of 0° E, are interpolated onto the model mesh. The model has 20 vertical levels of uniform thickness terrain sigma coordinates, each representing 5 % of the water column. Forcing data including temperature, salinity and currents are defined at the model open boundaries, based on a yearlong climatology representing average conditions between 1990 – 2014, to represent present day conditions. Depth-resolved temperature, salinity and non-tidal current inputs are generated from the Atlantic Margin Model [75], [76] interpolated onto the FVCOM vertical mesh at the open boundary nodes. The tidal components (currents and elevation) have been generated from the TPXO global ocean tidal model [77], with eight primary (M2, S2, N2, K2, K1, O1, P1, Q1), two long period (Mf, Mm) and 3 non-linear (M4, MS4, MN4) harmonic constituents from a single year interpolated onto the FVCOM mesh at each of the open boundary nodes. Surface forcing (wind, heating, precipitation) is derived from ECMWF ERA-Interim model configured for the UK shelf [78]. River freshwater data is sourced from Grid 2 Grid (1962-2011) obtained from the Centre of Ecology (CEH) [79], [80].

The hydrodynamics in the Scottish Shelf Model domain was run for a full year, with outputs recorded at the boundaries of both smaller domains in Figure 5b and Figure 5c, providing the nested forcing data. For the Goldeneye domain (Figure 5c) this forcing data was interpolated vertically to increase the resolution from 20 vertical layers to 100 vertical layers to give a vertical resolution in the same order of the horizontal resolution.

Initial conditions for the nested domains are taken from the state of the Scottish Shelf Model in Figure 5a, interpolated to the nested mesh removing the requirement for a long spin up time. However, a spin up time of 5-6 months is provided to ensure a quasi-steady state is reached.

In this study, the BDP in the PLUME model is CO_2 bubbles, where thermal properties such as density and solubility, along with transportation parameters such as, effective mass transfer, k_o in Eq. (3) and drag coefficient, c_d in Eq. (5) are all calculated by sub-models in the PLUME model. Details can be found from the previous publication [25]. The initial bubble properties are taken from the experiments presented in Sections 2.1 and 2.2, and the background seawater DIC concentration is predicted across the model domain through FVCOM-ERSEM [18], [29], with background TA and DIC kept constant based on experimental measurements also described in Sections 2.1 and 2.2.

The CO_2 bubbles are released from the seabed at the rates, sizes and positions described in Section 2 through the PLUME model. The bubbles travel within the model through interactions with the oceanic turbulent flows predicted from FVCOM, whilst dissolving. The CO_2 solution disperses in the turbulent ocean, meanwhile, outputs concentrations to the carbonate system in ERSEM to predict the changes in pH and pCO2.

This approach is an extension to that developed previously, where either a small scale multiphase model was used, but unable to cope with the complex hydrodynamics of the tidal cycle or long term leakages providing great limitations on the results [25]–[27], or a multi-scale, multi-phase system that due to its structured mesh design, struggles with coastline flows [35], [36]. The modelling system by Blackford et al. [18] and Cazenave et al. [29] nested ERSEM with FVCOM through the Framework for Aquatic Biogeochemical Models (FABM), assuming the gas plume and multi-phase aspects can be neglected by only considering the fully dissolved CO_2 solution in the first layer or applying a crude parameterisation of dissolution over a small number of bottom layers [14]. These assumptions are acceptable for large scale analysis, but for the prediction of dynamics local to the leakage areas,

such as these experiments, the bubbles and bubble plume dynamics play a larger role as shown by Dewar et al. [25]–[27].

4. Modelling System Results

The following sections investigate the fate of the CO_2 in both experiments described in Section 2 by exploring and quantifying the fate of both the gas bubble plume and the dissolved solution, which is advected within the model domains leading to an increase in acidity by increase in pCO_2 or decrease in pH of the seawaters when compared with background levels.

4.1. QICS

4.1.1. CO_2 Bubble Plume

The resultant bubbles from the PLUME model of the QICS experiment can be seen in Figure 6, a-c for each major injection rate given in Figure 2c, which can be compared with results from a Eulerian-Eulerian model by Dewar et al. presented in 2015 [25]. The bubbles in both models all rise and dissolve within ~10 m, with the average dissolution height of 4.1 m from PLUME, and maximum plume height recorded of 100 % of the water depth, compared to that of a maximum rise height of 88 % of the water depth by 2015 model [25]. It has to be noted that the minimum bubble size is set the same (0.01 mm) and the same sub-models of drag force and mass transfer are applied in both models to standardise the bubble physics.

4.1.2. Seawater pCO_2

The CO_2 solution plume, presented as pCO_2, from the PLUME modelling system can be seen in Figure 7a-c for each major injection rate. In this shallow mixed water column region, the solution is still largely confined to the lower water column, with the greatest penetration into the water column occurring in the vicinity of the release site around the bubble stream. The tides then advect the CO_2 solution away from the bubble plumes and disperse in the water column, as shown in Figure 7a-c, Figure 8a and b, with the affected volumes and seabed areas by increases in pCO_2 above the background value of 390 µatm.

Note that the values discussed in this study on pCO_2 are those of absolute value, and not changes in pCO_2 (ΔpCO_2) This is for convenience to compare with those from observations. Thresholds were set at pCO_2 of 500, 800 and 1600 µatm, where the range of impacted volumes and seabed areas at the highest leakage rate are also presented in Table 2. It can be seen that the majority of the perturbation is below 500 µatm, with affected volumes and seabed areas found to be a maximum of 3300 m^3 and 2528 m^2 respectively, with very small volumes (~292 m^3) and areas (~457 m^2) experiencing peaks exceeding 1600 µatm.

The release impact in the vertical is shown in Figure 9a, with the plume height of each threshold (pCO_2 of 500, 800 and 1600 µatm) plotted within the model domain for each time point in Figure 8c, and against the maximum height that the bubble plume reached. This shows that the release impact is mostly confined to the lower depths. However, some of the low pCO_2 impacts at peak release rates almost reach the sea surface (9.22 m at 500 µatm), at times exceeding the height of the bubble plume, from tidal contributions and turbulent diffusion in the vertical transportation of the CO_2 solution. In the horizontal, the length of the plume from the source to the tip for pCO_2 thresholds of 500, 800 and 1600 µatm is analysed across the simulation, with the spatial extents confined to within 101 m, 88 m, and 69 m from the release point, respectively as shown in Figure 8d.

4.2. *STEMM-CCS*

4.2.1. Bubble Plume

Bubbles from the STEMM-CCS experiment simulated by the PLUME model are presented in Figure 10a-d for each major injection rate given in Figure 3c. All the bubbles rise and dissolve within an average terminal height of 4.8 m, with the maximum height recorded as up to 25.1 m, or 21 % of the water depth when the largest (29 mm) bubble is released.

Table 2. Range of impacted volumes and areas at the highest leakage rate in the QICS experiment

pCO_2 (µatm)	Volume (m^3)	Area (m^2)
500	0 – 3300	0 – 2528
800	0 – 910	0 – 934
1600	0 – 292	0 – 457

4.2.2. Changes in seawater pH

The following section explores and quantifies the fate of changes in pH in seawater, governed by both the dissolution of CO_2 and the turbulent transportation. The changes in pH on the seafloor, predicted from the simulations are provided in Figure 11a-c for each major injection rate. Note, in contrast to the QICS experiments, the change in pH (ΔpH) is used for the STEMM-CCS experiment analysis as to match those of observations. The details of the solution plume impact volumes and the areas on the seafloor in terms of changes in pH in seawater are analysed and the results are given in Figure 12a and b by a decrease in pH from the background value of 8.04. Thresholds were set at -0.1, -0.3 and -0.6 units, where the range of impacted volumes and seabed areas at the highest leakage rate are also presented in Table 3.

The affected volumes and seabed areas are found to be up to a maximum of 7283 m^3 and 682 m^2 respectively at the threshold of -0.1. These impact volumes and areas shrink at a rate of order of magnitudes when analysing the changes upwards of -0.3 and -0.6 close to the seep source, with acute impacts only in the vicinity of the seep.

The release impact in the vertical is shown in Figure 9b, with the depth of each threshold (pH change of -0.1, -0.3 and -0.6) plotted within the model domain for each time point in Figure 12c, and against the maximum height that the bubble plume reached, showing that the release impact is mostly confined to the lower depths of <3 meters (pH change of -0.1 upwards). The stratified waters and the small vertical convection prevent further vertical movement in the timeframe of the experiment. In the horizontal, the length of the plume from the source to the tip for pH change thresholds of -0.1, -0.3 and -0.6, with the spatial extents confined to 94 m, 52 m, and 23.7 m from the release point, respectively as shown in Figure 12d.

5. Discussion

The simulations of the two field experiments presented in the last section show some specific findings for bubble and solution plumes from the different experimental designs outlined in Section 2 and Table 1. Discussions on those specifics are made in this section in attempting to understand the mechanisms and the physics behind the field observations.

It should be clarified before the discussion that the maximum impacts (pCO_2 increase or pH reduction) are sensitive to the leakage rates and the spatial distributions of seeps. Given that the QICS experiment is deeper into the sediments than in the STEMM-CCS experiment (15 m compared to 3 m), the observations show that there is greater horizontal movement of the gas prior to seepage. This provides the larger spatial distribution and footprint into the water column, which can be identified in Figure 2b and Figure 3b. An effect from this is that more seeps are created in the QICS experiment, reducing the leakage rate per seep, and in turn the local changes in dissolved CO_2 concentrations.

The bubble size distributions affect the changes in pH and pCO_2, due to fact that smaller bubbles under a given leakage flux can dissolve quicker than large bubbles because of the lager total interfacial area of the larger number of small bubbles. Differences in bubble sizes distributions reflect different geoformations (the geo-structure in sediments, such as the size and distribution of the micro fractures), and the oceanic current characteristics in turbulent bottom boundary layers. On the other hand, field observation methods and data treatments also play a certain role. Data from the QICS experiment are manually measured [28] from a single camera at 30 frames per second with a noisy background, creating uncertainties. This was overcome in the STEMM-CCS experiment, where measurements were automated, by using two underwater cameras at 90 frames per second in custom housings opposite an illuminated scale board. It is therefore considered that the distribution found in the STEMM-CCS is more representative, given the 8163 data points [49] shown in Figure 3a far exceeding the 345 data points from the QICS experiment [28] in Figure 2a. They are implemented into the model for each experiment respectively.

Table 3. STEMM-CCS range of impacted volumes and areas.

ΔpH	Volume (m^3)	Area (m^2)
-0.1	0 – 7283	0 – 682
-0.3	0 – 1225	0 – *193*
-0.6	0 – 401	0 – 56

In general, as presented in Sections 4.1 and 4.2, the model simulations are able to provide both CO_2 bubble and solution plume developments matching data found during both experiments, with further analysis below. One specific outcome from the model simulations is that they showed what was observed in both experiments, where the CO_2 solution accumulates at the release locations during low current speeds.

Modelling of CO_2 solution transportation shows that for both cases most of the release remains in the bottom of the waters, and the progression into the upper reaches of the water column is effectively prevented. This is recognized for both experiments, the well mixed water column in the QICS experiment and the stratified water column in STEMM-CCS, as shown in Figure 9. However, the dissolved solution plume can exceed the bubble plume height when the leakage is at higher rates, with buoyancy of the gas pushing and the drag force lifting the dissolved solution upwards along with vertical convection. These findings may also reflect the effect of vertical distribution of seawater density; in the QICS experiment the water is well mixed, however in the STEMM-CCS experiment stratification is present. Both simulations used hydrodynamic climatology and therefore some of the details of the localised mixing and stratification will be lost. The horizontal tidal currents seem to not transport the CO_2 very far from the release site. As seen in both experiments, the impacts extend not much further than ~100 m. What is shown from the simulations is that the shape and movements of the solution plume for these very small-scale experiments are mostly controlled by the local tides, confining the horizontal impacts to the vicinity of the leak. Larger and longer leaks have been shown to spread more significantly [14].

From the simulations it is also identified that the subsequent effect of these tidal currents is that although the plume appears to be a long narrow strip when flowing along the major axis of the tide, it circles with the tide, constantly changing, expanding the coverage and impacted area over the tidal cycle, and duration of the experiments, as shown in Table 4 and Figure 13, with fluctuating pH changes and pCO_2 measurable within the region over the CO_2 solution plumes.

Note that the high levels occur very briefly at the high leakage rate and are unlikely to be measurable in the field observations unless the sensor has a sufficient response time, and is in the correct place at the correct time, which is highly unlikely within the footprint of a reservoir complex in the order of kilometres.

5.1. QICS

The QICS experiment is simulated in full, over the 37 days by the PLUME model, with instantaneous hourly outputs. Therefore it provides a far larger data set than the 2015 model [25] that provided data over only 4 hours of simulated time. The Lagrangian scheme used in the PLUME model is also more suited in tracking bubbles than that of Eulerian scheme in the 2015 model [25], which integrates the particle differential equations over the grid volume, so can be highly resolution dependant. On the other hand, the oceanic turbulent flows can be better simulated by FVCOM, especially modelling of tides and ocean surface, than that in the small-scale turbulent ocean simulations [25], providing more dynamic seawater physics.

The discrepancies in the findings between these models may be understood through two major factors, the leakage rate, and a flooding / ebb tidal effect. For modelling of the CO_2 solution plumes, the 2015 model [25], with assumption of a 15% leakage rate based on a single measurement, predicts a maximum pCO_2 of 445 µatm, matching the mean pCO_2 measured in the experiment at 30 cm height, between 390 and 500 µatm [13]. This high-resolution model, however, is unable to reach the peak values experienced at 3cm from the seabed in the experiment (1600 µatm [40], [45]). Even assuming a 100% leakage rate, the highest pCO_2 in the water column from the model simulations is 713 µatm [25], less than half of observation.

Table 4. Impacted seabed areas from model simulations, showing the increased coverage of the plume over the duration of the experiment for QICS and STEMM-CCS.

QICS pCO_2 (µatm)	Maximum Instantaneous Area[1] (m^2)	Area over the entire experiment (m^2)
500	2528	19869
800	934	6918
1600	457	2244

STEMM-CCS ΔpH	Maximum Instantaneous Area[2] (m^2)	Area over the entire experiment (m^2)
-0.1	682	7237
-0.3	193	543
-0.6	56	60

The PLUME based model system implements the leakage rate data based on the acoustic measurements shown in Figure 2c, where the leakage rate is irregular and fluctuates with the tide about the 15% single physical leakage rate (shown by the red star). At times the acoustic leakage rate measurement may have been overestimated by background noise from ships and other users of the bay [42] being incorrectly calculated as bubbles. This would explain why some of the localised pCO_2 results from the PLUME based modelling system for the QICS experiment exceed those measured and highlights the difficulties and unknowns when extracting in-situ measurements in a complex and novel experiment.

The role of the tide on the dynamic developments of the solution plume are well simulated by the PLUME based modelling system, as shown in Figure 7 a-c at selected stages of the tidal cycle. The periodic movements [48] of the solution over the leakage source lead to an enhancement of the concentration of CO_2 solution from convective transportation, rather the turbulent diffusion. This mechanism momentarily increases CO_2 concentrations during the high and low tide points beyond what was predicted by the 2015 model [25], providing a more accurate understanding of the peak measurements, and analysis of the leak. This also confirms the mechanisms discussed by Dean et al. [17] and Cazenave et al. [29].

Further models were proposed and applied to the QICS project. The model proposed by Maeda et al. [48] is a single phase model focusing on the predictions of CO_2 solution dispersion by setting the ΔpH value as input data to the model for visualization of the CO_2 solution distribution without modelling of bubble dynamics.

The other model involved in the project, by Mori et al. [35], is most similar to the PLUME modelling system in this study, analysing multi-phase and multi-scale dynamics by taking into account the local hydrodynamics impact on the local plumes. The main differences between these models are that the one presented in this study has a smoother coastline from the use of an unstructured grid model at a slightly higher horizontal resolution, but a vertical resolution ~3 times higher to capture the details on the seabed found in the experimental measurements. However, the local sea loch has been neglected to simplify the hydrodynamics.

Mori et al. [35] also investigated dissolved phase release from sediments. Assuming a 17% dissolved solution release, Mori et al. [35] found a change of pCO_2 of ~100 µatm (~500 µatm total). This is close to the upper end of the mean pCO_2 measured at 30 cm height in the experiment, of between 390 and 500 µatm [13]. Increasing to 67% released as dissolved phase (so 75% of the injection rate), the pCO_2 reaches some of the high values experienced in the experiment at 3cm height, exceeding 1000 µatm. However, it is stated by Mori et al. [35] that measurements have shown that fluxes of dissolved solution across the sea-floor were negligible. Therefore, in this study, this additional release of dissolved solution from the sediment is not considered in model simulations.

It appears from the PLUME based modelling systems simulations, that the resolution local to the leakage source plays the key role, with the pCO_2 or pH calculated through the concentration of CO_2 solution, which is highly resolution dependent. In this study, the vertical resolution is almost three times higher, ~45 cm versus 1.3 m. The modelling results presented in section 4.2.2, approach the observation data, where due to the rapid dissolution of bubbles, and the dense solution sinking down to the seabed around the leakage source, a large increase in pCO_2 was measured at 3 cm height from the seabed, and was not recorded at 30 cm from the seabed [40], [45].

Both models use a very similar gas leakage rate prediction. However, the model by Mori et al. [35] used a

[1]the largest area at a single given time

filtered approach removing background noise fluctuations from their predictions. The unfiltered leakage rates used in this study may lead to some overprediction on the impacts, with the impacted areas at times being noticeably greater than that observed in the experiment, where the peaks of up to 1600 µatm were only measured briefly at 3cm above the seabed [40], [45]. The effect from not including a sea loch south of the release experiment that Mori et al. [35] suggests is required in accurately modelling the tidal current may also have impacted this.

5.2. *STEMM-CCS*

In the STEMM-CCS experiment, the bubble plume from the model simulations provides a reasonable match to experimental findings, where no bubbles were captured by the ROV above 8 meters from the seabed [41]. There are several considerations that will affect these figures. The first is the minimum bubble size that can be numerically modelled is 0.01 mm, which is 100 times less than the minimum bubble size detectable by the HD cameras at a meter distance from the bubble plume. Next is the initial bubble size distribution obtained from experiment observations from a single pockmark over a 15 minute period [41]. Therefore, this data set may only partially represent the bubble plume over 2 weeks, with up to 22 pockmarks over the entire experiment seen in Figure 3b. Another factor is the potential breakup of the larger bubbles into smaller bubbles [28] reducing the maximum plume height that is shown in the model to closer to the mean rise height. Bubble collisions have not been considered as there were limited recordings in the experiment from the dilute bubble plumes.

In the stratified water column, the impacts of the CO_2 release are even more confined to the lower water column than in the QICS experiment, with the greatest penetration occurring in the vicinity of the release site around the bubble stream. A further uncertainty lies with the leakage rate data, as discussed above, which was determined through gas collection and sampling techniques as the acoustic methods were highly affected by the background noise. This limited the measurement to 23 samples of a single bubble stream, providing a degree of uncertainty of the leakage rate over the experiment.

The results from Figure 12a and b, along with Table 3 are compared with STEMM-CCS experiment lab on chip sensors, which experienced a pH reduction of up to 0.6 and 0.3 units as peaks ~2.6 m downstream of the plume at 16.4 cm and 88 cm height from the seabed respectively, with average reductions of ~0.2 and 0.07 units during the largest leakage rate at those heights. Comparing with a COMSOL model simulating the STEMM-CCS experiment [81], pH changes over 0.1 and 0.01 affected volumes of 17 m^3 and 1024 m^3 respectively. Although these seem quite a bit lower than the values found in the ranges in Table 3, these were predicted using a single current [81] and therefore neglect the tidal accumulation shown in this study. All these values provide a reasonable comparison to the experimental findings and show how the concentration varies in the vertical, and the effects of resolution and tide on the PLUME modelling system.

5.3. *Modelling System Constraints*

The bubble plume is essential to produce the initial distribution of the dissolved solution in high resolution models. In the PLUME model for both experiments, the mean bubble plume distribution and rise heights are accurately predicted. However, the usefulness of the PLUME modelling system depends on the set up and resolution of the hydrodynamic model as the CO_2 bubbles dissolve very quickly in the water column.

Additionally, the forcing and regeneration of turbulent ocean through the regional ocean model should be carefully performed for assimilations of field experiments. As the Scottish Shelf Model is based on climatology forcing data (mean data from 1990 – 2014), some of the short-term high-resolution details of fluctuations in seawater properties, including mixing and stratification layers are likely to have been lost, which could impact on the experiment simulations as they are both very localised and only occur over relatively short timeframes of less than 40 days. These results can therefore only be taken as a prediction of the impact with some uncertainty rather than an attempt at an exact match to the experimental data.

Regarding the effects of a sea loch south of the bay [35] in the model simulations, the investigation from Taylor et al. [82] suggests that the thin stratified surface layer would not have an impact on the findings as the high pCO_2 changes are on the seabed, and the stratification only occurs in the surface layer (2-5 meters depth). Comparing the M2 dominant tidal ellipses in the model with Taylor et al. [82], they are the same shape, order and direction. However, the increases of kinetic energy would have an effect, with the internal waves produced, which were witnessed near the experiment site, contributing to greater mixing and explains why larger concentrations of pCO_2 are experienced within the model presented in this study.

6. Conclusions

The effect of localised hydrodynamics and bubble plume within simulations of CO_2 release or leakage in coastal waters are investigated through simulations of both the QICS and STEMM-CCS in-situ experiments using a new hydrodynamic and biogeochemical coupled modelling system incorporating FVCOM for local and regional hydrodynamics, and PLUME developed within this study as a two-way bubble plume model, which also linked to the carbonate system from ERSEM.

The results from this modelling system show that to a great extent anomalies in detectability and environmental impact findings from the first controlled sub-seabed release experiments of CO_2 (QICS and STEMM-CCS) have been resolved. Beyond the experiments within this study, the modelling system combined with knowledge of natural variability, can be used to quantify potential leakage impacts for a range of hypothetical scenarios and provides evaluation of leakage tracers allowing the derivation of highly sensitive anomaly indicators which might arise from leakage in order to facilitate detection, assurance and quantification relevant to carbon credits or potential damages and liability.

Dilution and dispersion from over a far longer period than the experimental timeframes would provide buffering, including transportation into deeper waters and surface water to air CO_2 exchange. This would impact larger scale leakages, but not on the scale of the experiments analysed within this paper, which represent a bubbly flow of a slow seep from a well or fault.

This paper, and results within, show that the newly developed extensive hydrodynamic and ecosystem modelling system, coupling the physics of local currents, tides, weather, bathymetry, with the physics of the bubble plume, significantly increases the accuracy of small-scale CO_2 leakage simulations, including the use of a Lagrangian approach for the bubble plume, and analysing the temporal high pCO_2 and pH change values from tidal impacts on the local dynamics. This model can be further applied for impact analysis by upscaling the PLUME model to investigate larger scale leakage scenarios, or for further development of CCS monitoring strategies [29], [83].

To fully understand the potential leakage mechanism of CO_2 gas and solution from the sediments, it is clear that more research and investigations are required on model developments based on the physics observed from both laboratory and in-situ experiments.

Acknowledgements

The authors were supported by the European Union's Horizon 2020 research and innovation programme under grant agreement No.654462 (STEMM-CCS) and the UK Research and Innovation National Environmental Research Council (UKRI-NERC) National Capability funding program CLASS (NE/R015953/1). This work is also part of the project ACTOM, funded through the ACT programme (Accelerating CCS Technologies, Horizon 2020 Project No 294766). Financial contributions made from: The Research Council of Norway, (RCN), Norway, Netherlands Enterprise Agency (RVO), Netherlands, Department for Business, Energy & Industrial Strategy (BEIS) together with extra funding from NERC and EPSRC research councils, United Kingdom, US-Department of Energy (US-DOE), USA. In-kind contributions from the University of Bergen are gratefully acknowledged. The authors also acknowledge the Research Council of Norway through the CLIMIT program funded project no 254711 (Baymode).

Generation of model inputs for FVCOM used the FVCOM MATLAB toolbox [84]. With colour maps, graphs and figures produced by MATLAB [85].

References

[1] R. K. Pachauri et al., Climate change 2014: synthesis report. Contribution of Working Groups I, II and III to the fifth assessment report of the Intergovernmental Panel on Climate Change. IPCC, 2014. Accessed: Jul. 17, 2017. [Online]. Available: https://epic.awi.de/37530/

[2] M. R. Raupach et al., "Global and regional drivers of accelerating CO2 emissions," Proc. Natl. Acad. Sci., vol. 104, no. 24, Art. no. 24, Jun. 2007, doi: 10.1073/pnas.0700609104.

[3] B. Metz and Intergovernmental Panel on Climate Change, Eds., IPCC special report on carbon dioxide capture and storage. Cambridge: Cambridge University Press, for the Intergovernmental Panel on Climate

Change, 2005.
[4] J. Sumner, L. Bird, and H. Smith, "Carbon Taxes: A Review of Experience and Policy Design Considerations," Tech. Rep., p. 38, 2009.
[5] O. Edenhofer and Intergovernmental Panel on Climate Change, Eds., Climate change 2014: mitigation of climate change: Working Group III contribution to the Fifth assessment report of the Intergovernmental Panel on Climate Change. New York, NY: Cambridge University Press, 2014.
[6] Y. Artioli et al., "Heterogeneity of impacts of high CO_2 on the North Western European Shelf," Biogeosciences, vol. 11, no. 3, pp. 601–612, Feb. 2014, doi: https://doi.org/10.5194/bg-11-601-2014.
[7] M. Barange et al., "Predicting the Impacts and Socio-Economic Consequences of Climate Change on Global Marine Ecosystems and Fisheries," in World Fisheries, John Wiley & Sons, Ltd, 2011, pp. 29–59. doi: 10.1002/9781444392241.ch3.
[8] T. Dixon, S. T. McCoy, and I. Havercroft, "Legal and Regulatory Developments on CCS," Int. J. Greenh. Gas Control, vol. 40, pp. 431–448, Sep. 2015, doi: 10.1016/j.ijggc.2015.05.024.
[9] J. A. Bradbury, "PUBLIC UNDERSTANDING OF AND ENGAGEMENT WITH CCS," The Social Dynamics of Carbon Capture and Storage, May 04, 2012. https://www.taylorfrancis.com/ (accessed Aug. 07, 2019).
[10] "Carbon sequestration: Buried trouble : Nature News." Accessed: Aug. 07, 2019. [Online]. Available: https://www.nature.com/news/2010/100217/full/463871a.html
[11] R. Monastersky, "Seabed scars raise questions over carbon-storage plan," Nat. News, vol. 504, no. 7480, Art. no. 7480, Dec. 2013, doi: 10.1038/504339a.
[12] T. Dixon, S. T. McCoy, and I. Havercroft, "Legal and Regulatory Developments on CCS," Int. J. Greenh. Gas Control, vol. 40, pp. 431–448, Sep. 2015, doi: 10.1016/j.ijggc.2015.05.024.
[13] J. Blackford et al., "Detection and impacts of leakage from sub-seafloor deep geological carbon dioxide storage," Nat. Clim. Change, vol. 4, no. 11, Art. no. 11, Nov. 2014, doi: 10.1038/nclimate2381.
[14] J. Blackford et al., "Impact and detectability of hypothetical CCS offshore seep scenarios as an aid to storage assurance and risk assessment," Int. J. Greenh. Gas Control, vol. 95, p. 102949, Apr. 2020, doi: 10.1016/j.ijggc.2019.102949.
[15] Y. Shirayama and H. Thornton, "Effect of increased atmospheric CO2 on shallow water marine benthos," J. Geophys. Res. Oceans, vol. 110, no. C9, Art. no. C9, Sep. 2005, doi: 10.1029/2004JC002618.
[16] J. J. Roberts and L. Stalker, "What have we learnt about CO2 leakage from CO2 release field experiments, and what are the gaps for the future?," Earth-Sci. Rev., vol. 209, p. 102939, Oct. 2020, doi: 10.1016/j.earscirev.2019.102939.
[17] M. Dean, J. Blackford, D. Connelly, and R. Hines, "Insights and guidance for offshore CO2 storage monitoring based on the QICS, ETI MMV, and STEMM-CCS projects," Int. J. Greenh. Gas Control, vol. 100, p. 103120, Sep. 2020, doi: 10.1016/j.ijggc.2020.103120.
[18] J. C. Blackford, R. Torres, P. Cazanave, and Y. Artioli, "Modelling Dispersion of CO2 Plumes in Sea Water as an Aid to Monitoring and Understanding Ecological Impact," Energy Procedia, vol. 37, pp. 3379–3386, 2013, doi: 10.1016/j.egypro.2013.06.226.
[19] J. C. Blackford, N. Jones, R. Proctor, and J. Holt, "Regional scale impacts of distinct CO2 additions in the North Sea," Mar. Pollut. Bull., vol. 56, no. 8, Art. no. 8, Aug. 2008, doi: 10.1016/j.marpolbul.2008.04.048.
[20] J. C. Blackford and F. J. Gilbert, "pH variability and CO2 induced acidification in the North Sea," J. Mar. Syst., vol. 64, no. 1–4, Art. no. 1–4, Jan. 2007, doi: 10.1016/j.jmarsys.2006.03.016.
[21] J. Greenwood, P. Craig, and N. Hardman-Mountford, "Coastal monitoring strategy for geochemical detection of fugitive CO2 seeps from the seabed," Int. J. Greenh. Gas Control, vol. 39, pp. 74–78, Aug. 2015, doi: 10.1016/j.ijggc.2015.05.010.
[22] H. K. Hvidevold, G. Alendal, T. Johannessen, A. Ali, T. Mannseth, and H. Avlesen, "Layout of CCS monitoring infrastructure with highest probability of detecting a footprint of a CO2 leak in a varying marine environment," Int. J. Greenh. Gas Control, vol. 37, pp. 274–279, Jun. 2015, doi: 10.1016/j.ijggc.2015.03.013.
[23] J. J. C. Phelps, J. C. Blackford, J. T. Holt, and J. A. Polton, "Modelling large-scale CO2 leakages in the North Sea," Int. J. Greenh. Gas Control, vol. 38, pp. 210–220, Jul. 2015, doi: 10.1016/j.ijggc.2014.10.013.
[24] M. Dewar, "Modelling the two-phase plume dynamics of CO2 leakage into open shallow waters," Thesis, Heriot-Watt University, 2016. Accessed: Nov. 27, 2017. [Online]. Available: http://www.ros.hw.ac.uk/handle/10399/3093
[25] M. Dewar, N. Sellami, and B. Chen, "Dynamics of rising CO2 bubble plumes in the QICS field experiment: Part 2 – Modelling," Int. J. Greenh. Gas Control, vol. 38, pp. 52–63, Jul. 2015, doi: 10.1016/j.ijggc.2014.11.003.
[26] M. Dewar, W. Wei, D. McNeil, and B. Chen, "Simulation of the Near Field Physiochemical Impact of CO2 Leakage into Shallow Water in the North Sea," Energy Procedia, vol. 37, pp. 3413–3423, 2013, doi: 10.1016/j.egypro.2013.06.230.

[27] M. Dewar, W. Wei, D. McNeil, and B. Chen, "Small-scale modelling of the physiochemical impacts of CO2 leaked from sub-seabed reservoirs or pipelines within the North Sea and surrounding waters," Mar. Pollut. Bull., vol. 73, no. 2, Art. no. 2, Aug. 2013, doi: 10.1016/j.marpolbul.2013.03.005.
[28] N. Sellami, M. Dewar, H. Stahl, and B. Chen, "Dynamics of rising CO2 bubble plumes in the QICS field experiment: Part 1 – The experiment," Int. J. Greenh. Gas Control, vol. 38, pp. 44–51, Jul. 2015, doi: 10.1016/j.ijggc.2015.02.011.
[29] P. W. Cazenave et al., "Optimising environmental monitoring for carbon dioxide sequestered offshore," Int. J. Greenh. Gas Control, vol. 110, p. 103397, Sep. 2021, doi: 10.1016/j.ijggc.2021.103397.
[30] B. Chen, M. Nishio, Y. Song, and M. Akai, "The fate of CO2 bubble leaked from seabed," Energy Procedia, vol. 1, no. 1, Art. no. 1, Feb. 2009, doi: 10.1016/j.egypro.2009.02.329.
[31] R. E. Zeebe and D. A. Wolf-Gladrow, CO2 in Seawater: Equilibrium, Kinetics, Isotopes. Gulf Professional Publishing, 2001.
[32] Y. Song, M. Nishio, B. Chen, S. Someya, T. Uchida, and M. Akai, "Measurement of the Density of CO2 Solution by Mach-Zehnder Interferometry," Ann. N. Y. Acad. Sci., vol. 972, no. 1, Art. no. 1, Oct. 2002, doi: 10.1111/j.1749-6632.2002.tb04574.x.
[33] Y. Song et al., "Measurements of CO2–H2O–NaCl Solution Densities over a Wide Range of Temperatures, Pressures, and NaCl Concentrations," J. Chem. Eng. Data, vol. 58, no. 12, Art. no. 12, Dec. 2013, doi: 10.1021/je400459y.
[34] B. Chen, Y. Song, M. Nishio, S. Someya, and M. Akai, "Modeling near-field dispersion from direct injection of carbon dioxide into the ocean," J. Geophys. Res. Oceans, vol. 110, no. C9, Art. no. C9, Sep. 2005, doi: 10.1029/2004JC002567.
[35] C. Mori et al., "Numerical study of the fate of CO2 purposefully injected into the sediment and seeping from seafloor in Ardmucknish Bay," Int. J. Greenh. Gas Control, vol. 38, pp. 153–161, Jul. 2015, doi: 10.1016/j.ijggc.2014.11.023.
[36] Y. Kano, T. Sato, J. Kita, S. Hirabayashi, and S. Tabeta, "Multi-scale modeling of CO2 dispersion leaked from seafloor off the Japanese coast," Mar. Pollut. Bull., vol. 60, no. 2, Art. no. 2, Feb. 2010, doi: 10.1016/j.marpolbul.2009.09.024.
[37] C. Chen, H. Liu, and R. C. Beardsley, "An Unstructured Grid, Finite-Volume, Three-Dimensional, Primitive Equations Ocean Model: Application to Coastal Ocean and Estuaries," J. Atmospheric Ocean. Technol., vol. 20, no. 1, Art. no. 1, Jan. 2003, doi: 10.1175/1520-0426(2003)020<0159:AUGFVT>2.0.CO;2.
[38] Y. Artioli et al., "The carbonate system in the North Sea: Sensitivity and model validation," J. Mar. Syst., vol. 102–104, pp. 1–13, Oct. 2012, doi: 10.1016/j.jmarsys.2012.04.006.
[39] CH2M -, "The Scottish Shelf Model. Part 1: Shelf-Wide Domain: Scottish Marine and Freshwater Science Vol 7 No 3," 2016, doi: 10.7489/1692-1.
[40] D. Atamanchuk et al., "Detection of CO2 leakage from a simulated sub-seabed storage site using three different types of pCO2 sensors," Int. J. Greenh. Gas Control, vol. 38, pp. 121–134, Jul. 2015, doi: 10.1016/j.ijggc.2014.10.021.
[41] A. Flohr et al., "Towards improved monitoring of offshore carbon storage: A real-world field experiment detecting a controlled sub-seafloor CO2 release," Int. J. Greenh. Gas Control, vol. 106, p. 103237, Mar. 2021, doi: 10.1016/j.ijggc.2020.103237.
[42] B. J. P. Bergès, T. G. Leighton, and P. R. White, "Passive acoustic quantification of gas fluxes during controlled gas release experiments," Int. J. Greenh. Gas Control, vol. 38, pp. 64–79, Jul. 2015, doi: 10.1016/j.ijggc.2015.02.008.
[43] "QICS Data: Effect of a controlled sub-seabed release of CO2 on the biogeochemistry of shallow marine sediments, pore waters, and the overlying water (2012-2013)," NERC Data Catalogue Service. https://data-search.nerc.ac.uk/geonetwork/srv/api/records/0a6b0b4d-65a2-2bdb-e054-002128a47908 (accessed Aug. 09, 2021).
[44] J. Kita, H. Stahl, M. Hayashi, T. Green, Y. Watanabe, and S. Widdicombe, "Benthic megafauna and CO2 bubble dynamics observed by underwater photography during a controlled sub-seabed release of CO2," Int. J. Greenh. Gas Control, vol. 38, pp. 202–209, Jul. 2015, doi: 10.1016/j.ijggc.2014.11.012.
[45] K. Shitashima, Y. Maeda, and A. Sakamoto, "Detection and monitoring of leaked CO2 through sediment, water column and atmosphere in a sub-seabed CCS experiment," Int. J. Greenh. Gas Control, vol. 38, pp. 135–142, Jul. 2015, doi: 10.1016/j.ijggc.2014.12.011.
[46] J. Blackford et al., "Marine baseline and monitoring strategies for carbon dioxide capture and storage (CCS)," Int. J. Greenh. Gas Control, vol. 38, pp. 221–229, Jul. 2015, doi: 10.1016/j.ijggc.2014.10.004.
[47] A. Lichtschlag, R. H. James, H. Stahl, and D. Connelly, "Effect of a controlled sub-seabed release of CO2 on the biogeochemistry of shallow marine sediments, their pore waters, and the overlying water column," Int. J. Greenh. Gas Control, vol. 38, pp. 80–92, Jul. 2015, doi: 10.1016/j.ijggc.2014.10.008.
[48] Y. Maeda, K. Shitashima, and A. Sakamoto, "Mapping observations using AUV and numerical simulations of leaked CO2 diffusion in sub-seabed CO2 release experiment at Ardmucknish Bay," Int. J. Greenh. Gas

Control, vol. 38, pp. 143–152, Jul. 2015, doi: 10.1016/j.ijggc.2015.01.017.
[49] J. Li et al., "Acoustic and optical determination of bubble size distributions – Quantification of seabed gas emissions," Int. J. Greenh. Gas Control, vol. 108, p. 103313, Jun. 2021, doi: 10.1016/j.ijggc.2021.103313.
[50] A. Flohr et al., "Utility of natural and artificial geochemical tracers for leakage monitoring and quantification during an off-shore controlled CO2 release experiment," Int. J. Greenh. Gas Control, no. This issue.
[51] D. Koopmans et al., "Detection and quantification of a release of carbon dioxide gas from the seafloor using pH eddy covariance and mass transport," Int. J. Greenh. Gas Control, no. This Issue.
[52] A. Schaap et al., "Quantification of a subsea CO2 release with lab-on-chip sensors measuring benthic gradients," Int. J. Greenh. Gas Control, vol. 110, p. 103427, Sep. 2021, doi: 10.1016/j.ijggc.2021.103427.
[53] J. C. Blackford, J. I. Allen, and F. J. Gilbert, "Ecosystem dynamics at six contrasting sites: a generic modelling study," J. Mar. Syst., vol. 52, no. 1, pp. 191–215, Dec. 2004, doi: 10.1016/j.jmarsys.2004.02.004.
[54] M. Butenschön et al., "ERSEM 15.06: a generic model for marine biogeochemistry and the ecosystem dynamics of the lower trophic levels," Geosci. Model Dev., vol. 9, pp. 1293–1339, Apr. 2016, doi: 10.5194/gmd-9-1293-2016.
[55] W. Yao and C. Morel, "Volumetric interfacial area prediction in upward bubbly two-phase flow," Int. J. Heat Mass Transf., vol. 47, no. 2, Art. no. 2, Jan. 2004, doi: 10.1016/j.ijheatmasstransfer.2003.06.004.
[56] J. C. Blackford and P. H. Burkill, "Planktonic community structure and carbon cycling in the Arabian Sea as a result of monsoonal forcing: the application of a generic model," J. Mar. Syst., vol. 36, no. 3, pp. 239–267, Oct. 2002, doi: 10.1016/S0924-7963(02)00182-3.
[57] N. Ingri, W. Kakolowicz, L. G. Sillén, and B. Warnqvist, "High-speed computers as a supplement to graphical methods—V11Part IV—Arkiv Kemi, 1964, 23, 97; for commsnt on spelling 'program' see Talanta, 1967, 14, 833.: Haltafall, a general program for calculating the composition of equilibrium mixtures," Talanta, vol. 14, no. 11, pp. 1261–1286, Nov. 1967, doi: 10.1016/0039-9140(67)80203-0.
[58] C. Chen, H. Huang, R. C. Beardsley, H. Liu, Q. Xu, and G. Cowles, "A finite volume numerical approach for coastal ocean circulation studies: Comparisons with finite difference models," J. Geophys. Res., vol. 112, no. C3, Art. no. C3, Mar. 2007, doi: 10.1029/2006JC003485.
[59] J. Ge, P. Ding, C. Chen, S. Hu, G. Fu, and L. Wu, "An integrated East China Sea–Changjiang Estuary model system with aim at resolving multi-scale regional–shelf–estuarine dynamics," Ocean Dyn., vol. 63, no. 8, pp. 881–900, Aug. 2013, doi: 10.1007/s10236-013-0631-3.
[60] H. Huang, "Finite Volume Coastal Ocean Model (FVCOM) 3D Hydrodynamic Model Comparison," p. 43, May 2011.
[61] Z. Yang and T. Khangaonkar, "Modeling of Salt Intrusion, Intertidal Mixing, and Circulation in a Braided Estuary," J. Coast. Res., pp. 171–180, Jan. 2008, doi: 10.2112/1551-5036-52.sp1.171.
[62] L. Zheng and R. H. Weisberg, "Modeling the west Florida coastal ocean by downscaling from the deep ocean, across the continental shelf and into the estuaries," Ocean Model., vol. 48, pp. 10–29, May 2012, doi: 10.1016/j.ocemod.2012.02.002.
[63] P. W. Cazenave, R. Torres, and J. I. Allen, "Unstructured grid modelling of offshore wind farm impacts on seasonally stratified shelf seas," Prog. Oceanogr., vol. 145, pp. 25–41, Jun. 2016, doi: 10.1016/j.pocean.2016.04.004.
[64] M. De Dominicis, R. O'Hara Murray, and J. Wolf, "Multi-scale ocean response to a large tidal stream turbine array," Renew. Energy, vol. 114, pp. 1160–1179, Dec. 2017, doi: 10.1016/j.renene.2017.07.058.
[65] X. Li et al., "Three-dimensional modelling of suspended sediment transport in the far wake of tidal stream turbines," Renew. Energy, vol. 151, pp. 956–965, May 2020, doi: 10.1016/j.renene.2019.11.096.
[66] R. Torres and R. J. Uncles, "2.17 – Modeling of Estuarine and Coastal Waters," in Treatise on Estuarine and Coastal Science, vol. 2, 2011, pp. 395–427. doi: 10.1016/B978-0-12-374711-2.00216-3.
[67] D. Aleynik, A. C. Dale, M. Porter, and K. Davidson, "A high resolution hydrodynamic model system suitable for novel harmful algal bloom modelling in areas of complex coastline and topography," Harmful Algae, vol. 53, pp. 102–117, Mar. 2016, doi: 10.1016/j.hal.2015.11.012.
[68] J. J. Waggitt, P. W. Cazenave, L. M. Howarth, P. G. H. Evans, J. van der Kooij, and J. G. Hiddink, "Combined measurements of prey availability explain habitat selection in foraging seabirds," Biol. Lett., vol. 14, no. 8, p. 20180348, Aug. 2018, doi: 10.1098/rsbl.2018.0348.
[69] J. J. Waggitt, P. W. Cazenave, R. Torres, B. J. Williamson, and B. E. Scott, "Predictable hydrodynamic conditions explain temporal variations in the density of benthic foraging seabirds in a tidal stream environment," ICES J. Mar. Sci., vol. 73, no. 10, pp. 2677–2686, Nov. 2016, doi: 10.1093/icesjms/fsw100.
[70] J. J. Waggitt, P. W. Cazenave, R. Torres, B. J. Williamson, and B. E. Scott, "Quantifying pursuit-diving seabirds' associations with fine-scale physical features in tidal stream environments," J. Appl. Ecol., vol. 53, no. 6, pp. 1653–1666, 2016, doi: 10.1111/1365-2664.12646.
[71] T. P. Adams, R. G. Miller, D. Aleynik, and M. T. Burrows, "Offshore marine renewable energy devices as stepping stones across biogeographical boundaries," J. Appl. Ecol., vol. 51, no. 2, pp. 330–338, 2014, doi: 10.1111/1365-2664.12207.

[72] T. Adams, K. Black, C. MacIntyre, I. MacIntyre, and R. Dean, "Connectivity modelling and network analysis of sea lice infection in Loch Fyne, west coast of Scotland," Aquac. Environ. Interact., vol. 3, no. 1, pp. 51–63, Dec. 2012, doi: 10.3354/aei00052.
[73] Chen, An Unstructured-grid, Finite-volume Community Ocean Model: FVCOM User Manual (3rd Edition). Sea Grant College Program, Massachusetts Institute of Technology, 2013.
[74] M. De Dominicis, R. O. Murray, A. Gallego, and J. Wolf, "The Scottish Shelf Model 1990 – 2014 climatology 2.01," 2018, doi: 10.7489/12037-1.
[75] E. J. O'Dea et al., "An operational ocean forecast system incorporating NEMO and SST data assimilation for the tidally driven European North-West shelf," J. Oper. Oceanogr., vol. 5, no. 1, pp. 3–17, Feb. 2012, doi: 10.1080/1755876X.2012.11020128.
[76] K. P. Edwards, R. Barciela, and M. Butenschön, "Validation of the NEMO-ERSEM operational ecosystem model for the North West European Continental Shelf," Ocean Sci., vol. 8, no. 6, pp. 983–1000, Nov. 2012, doi: https://doi.org/10.5194/os-8-983-2012.
[77] G. D. Egbert and S. Y. Erofeeva, "Efficient Inverse Modeling of Barotropic Ocean Tides," J. Atmospheric Ocean. Technol., vol. 19, no. 2, pp. 183–204, Feb. 2002, doi: 10.1175/1520-0426(2002)019<0183:EIMOBO>2.0.CO;2.
[78] D. P. Dee et al., "The ERA-Interim reanalysis: configuration and performance of the data assimilation system," Q. J. R. Meteorol. Soc., vol. 137, no. 656, pp. 553–597, 2011, doi: 10.1002/qj.828.
[79] V. A. Bell, A. L. Kay, R. G. Jones, and R. J. Moore, "Development of a high resolution grid-based river flow model for use with regional climate model output," Hydrol. Earth Syst. Sci., vol. 11, no. 1, pp. 532–549, Jan. 2007, doi: https://doi.org/10.5194/hess-11-532-2007.
[80] S. J. Cole and R. J. Moore, "Distributed hydrological modelling using weather radar in gauged and ungauged basins," Adv. Water Resour., vol. 32, no. 7, pp. 1107–1120, Jul. 2009, doi: 10.1016/j.advwatres.2009.01.006.
[81] S. Monk et al., "Detecting and mapping a CO2 plume with novel autonomous sensors on an underwater remote-operated vehicle," Int. J. Greenh. Gas Control, vol. This Issue.
[82] P. Taylor et al., "A novel sub-seabed CO2 release experiment informing monitoring and impact assessment for geological carbon storage," Int. J. Greenh. Gas Control, vol. 38, pp. 3–17, Jul. 2015, doi: 10.1016/j.ijggc.2014.09.007.
[83] A. Oleynik, M. I. García-Ibáñez, N. Blaser, A. Omar, and G. Alendal, "Optimal sensors placement for detecting CO2 discharges from unknown locations on the seafloor," Int. J. Greenh. Gas Control, vol. 95, p. 102951, Apr. 2020, doi: 10.1016/j.ijggc.2019.102951.
[84] P. Cazenave, R. Torres, R. O'Hara Murray, K. Amoudry, and C. Liu, pwcazenave/fvcom-toolbox: Relatively minor fixes with improvements and bug squashing. Zenodo, 2019. doi: 10.5281/zenodo.2573959.
[85] MATLAB, 9.3.0.948333 (R2017b). The MathWorks Inc., 2017.

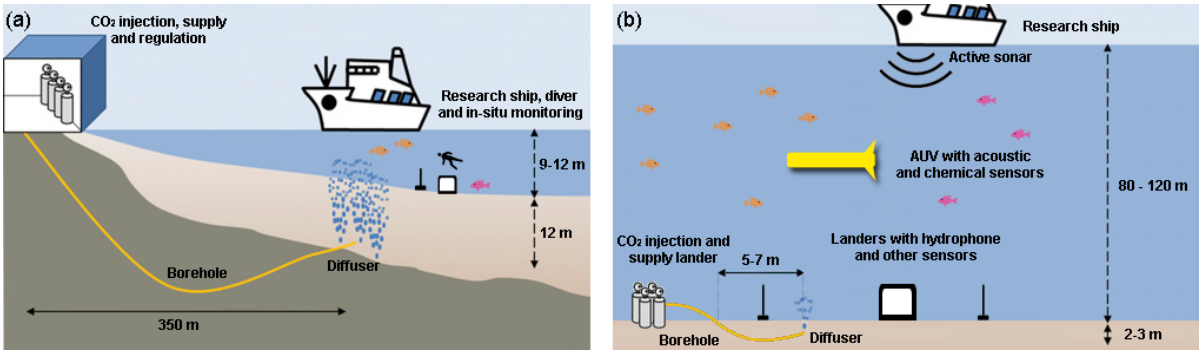

Figure 1. Graphical representations of the in-situ experimental setup (not to scale). a) The QICS experiment; b) The STEMM-CCS experiment.

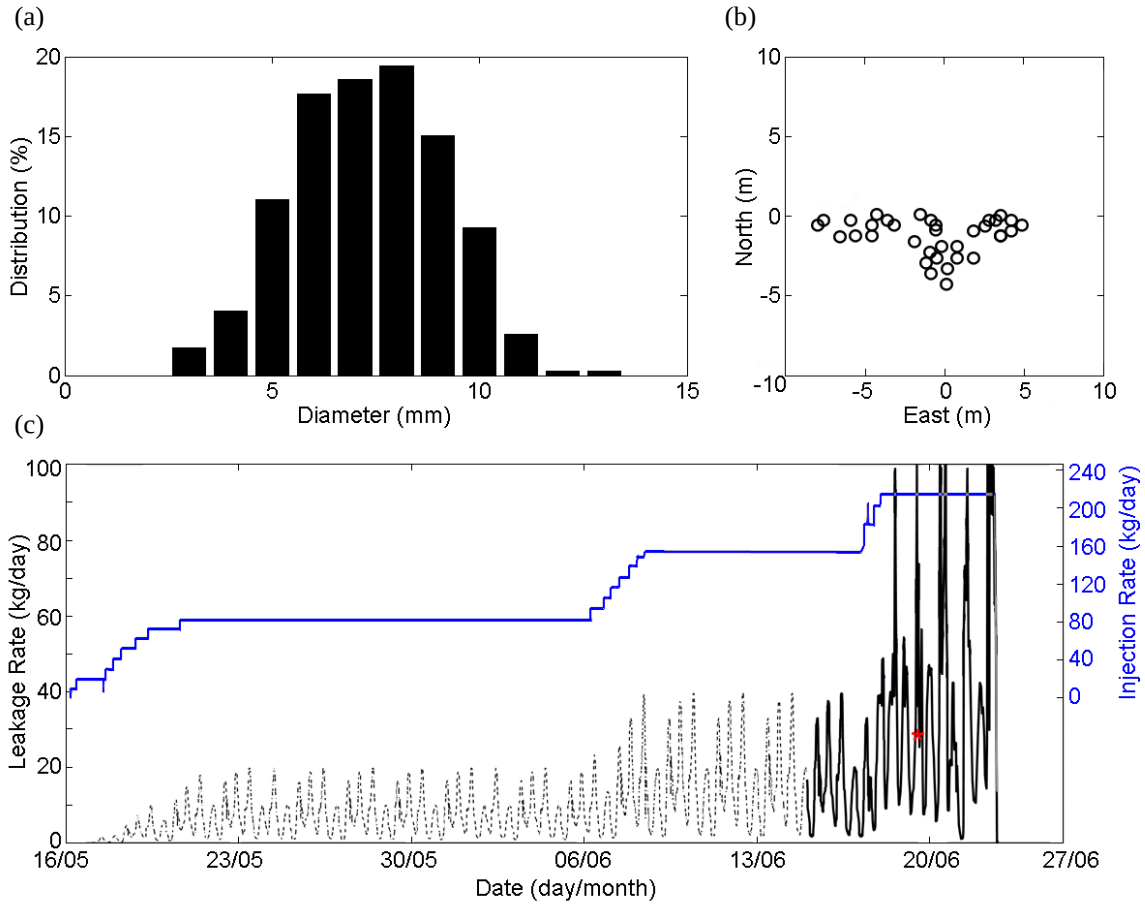

Figure 2. QICS experimental data. a) The bubble size distribution in terms of diameter, top left; b) The bubble stream pockmark locations, top right; c) The leakage rate measured acoustically (solid line) and extrapolated based on injection rate ratio of the measured data (dashed line), with the blue line showing the experiment injection rate and the red point shows the physical leakage rate measurement, bottom.

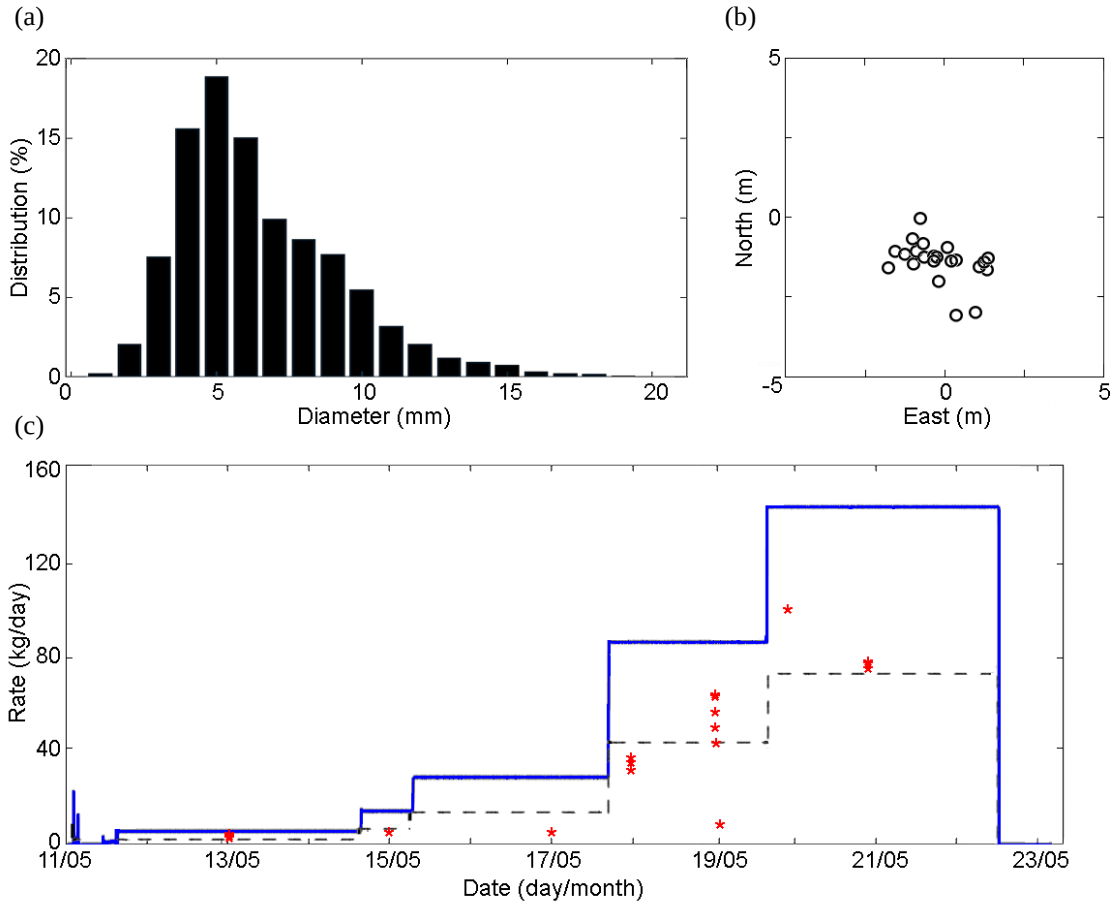

Figure 3. STEMM-CCS experimental data. a) The bubble size distribution in terms of diameter from 0-20 mm [49], top left; b) The bubble stream pockmark locations, top right; c) The leakage rate used in the model 50% of the injection rate based on the physical leakage rate measurements (dashed line), with the blue line showing the experiment injection rate and the red points show the physical leakage rate measurements, bottom.

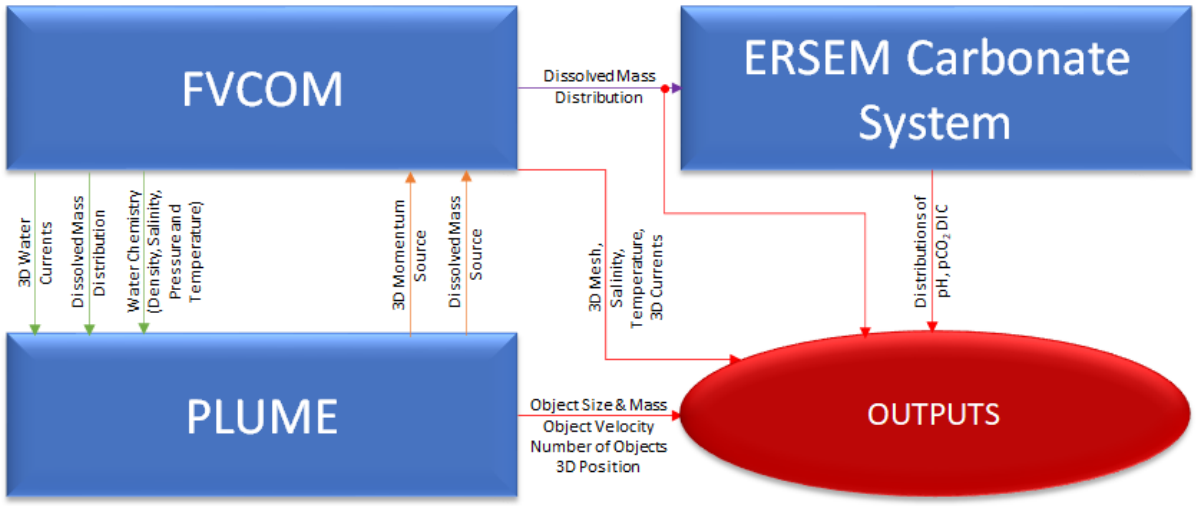

Figure 4. The modelling system interaction chart, showing how the models (PLUME, FVCOM, and ERSEM) interact with each other, and which variables are exchanged.

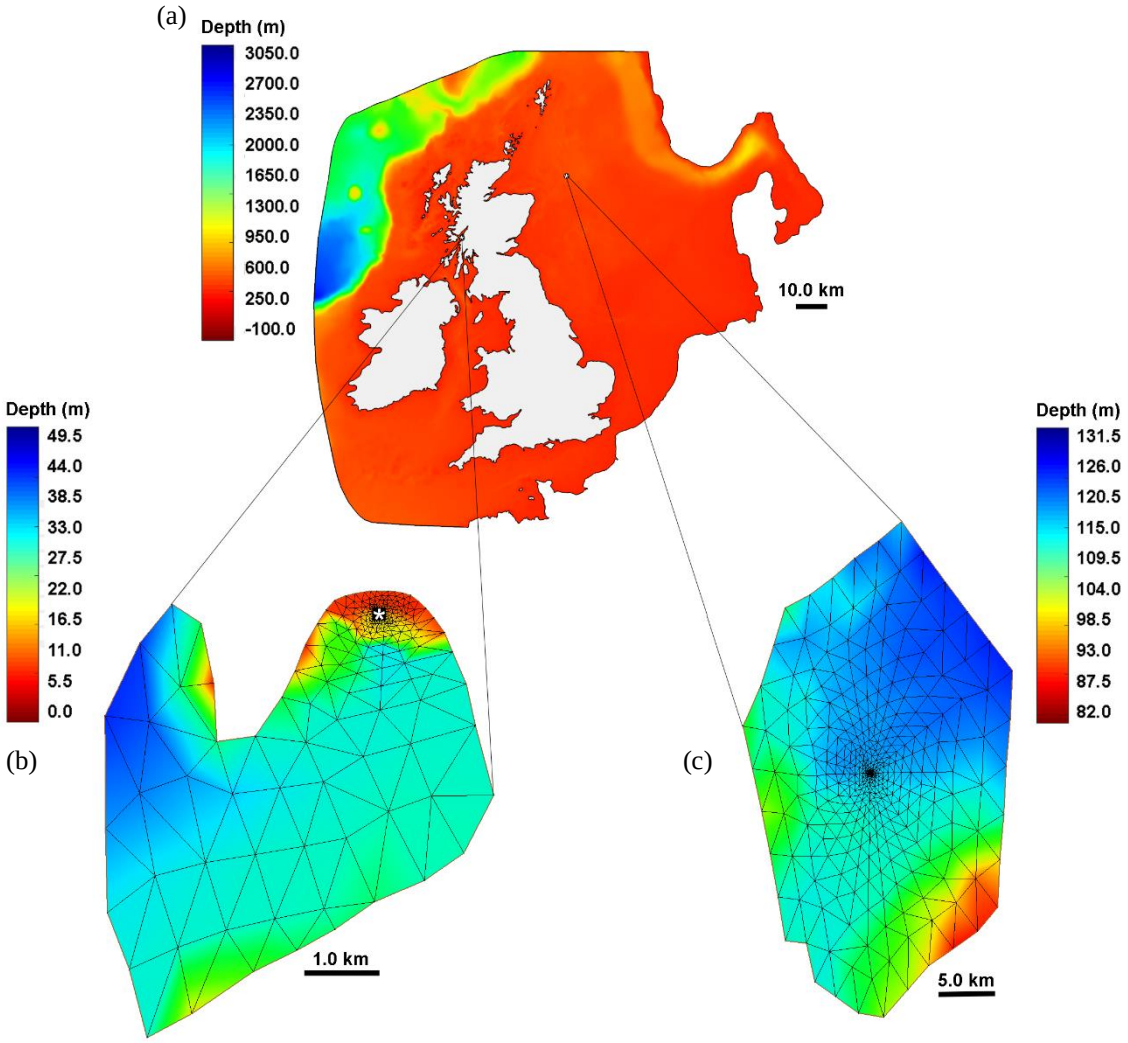

Figure 5. FVCOM model domains, contours represent the bathymetry depth, with a key colour bar for each domain and white stars representing the leakage sites. a) The Scottish Shelf Model, top; b) The QICS experiment, bottom left; c) The STEMM-CCS experiment, bottom right.

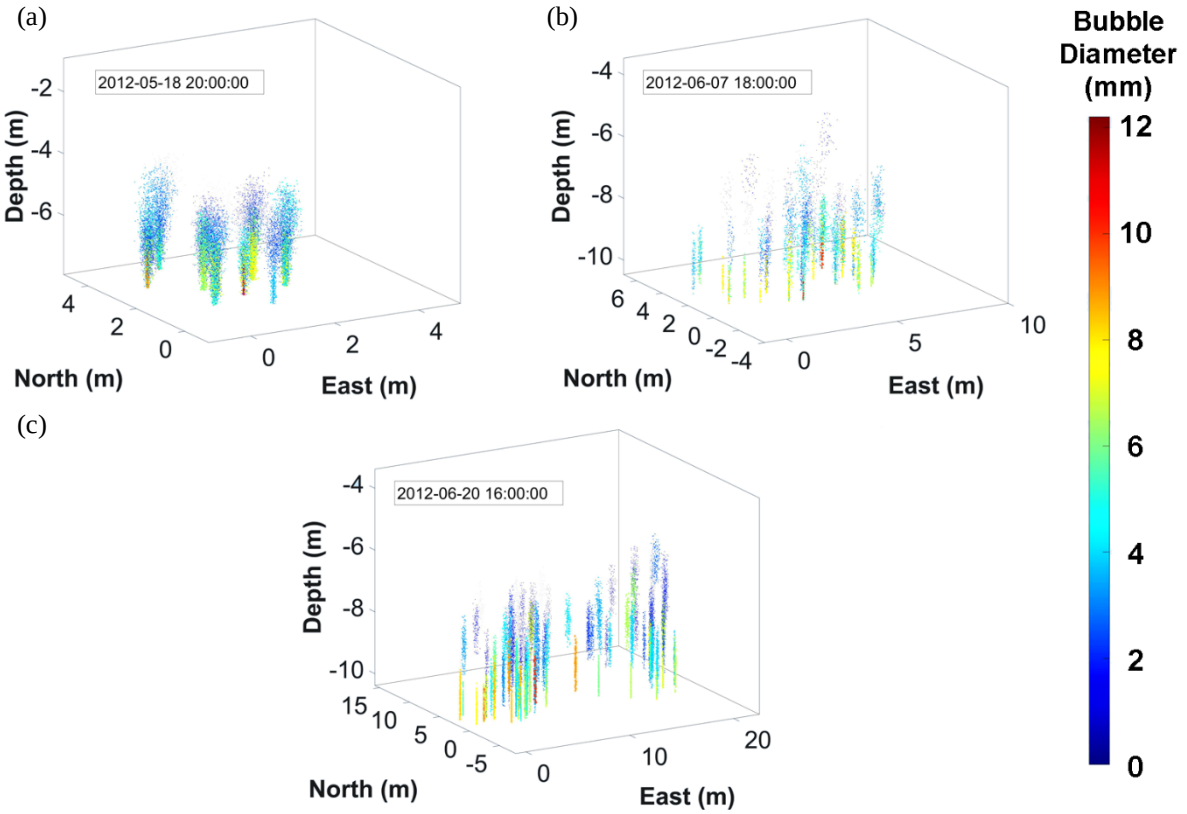

Figure 6. The bubble streams at various timestamps for the QICS experiment, with the bubble diameter (mm) shown by both the colour map and the size of the marker. a) The PLUME model at the low injection rate (80 kg/day on 18/05/2012) zoomed in to the 8 initial bubble streams, top left; b) The PLUME model at the middle injection rate (170 kg/day on 07/06/2012) zoomed in to the 20 active bubble streams, top right; c) The PLUME model at the top injection rate (208 kg/day on 22/06/2012), showing the full 35 active bubble streams, bottom.

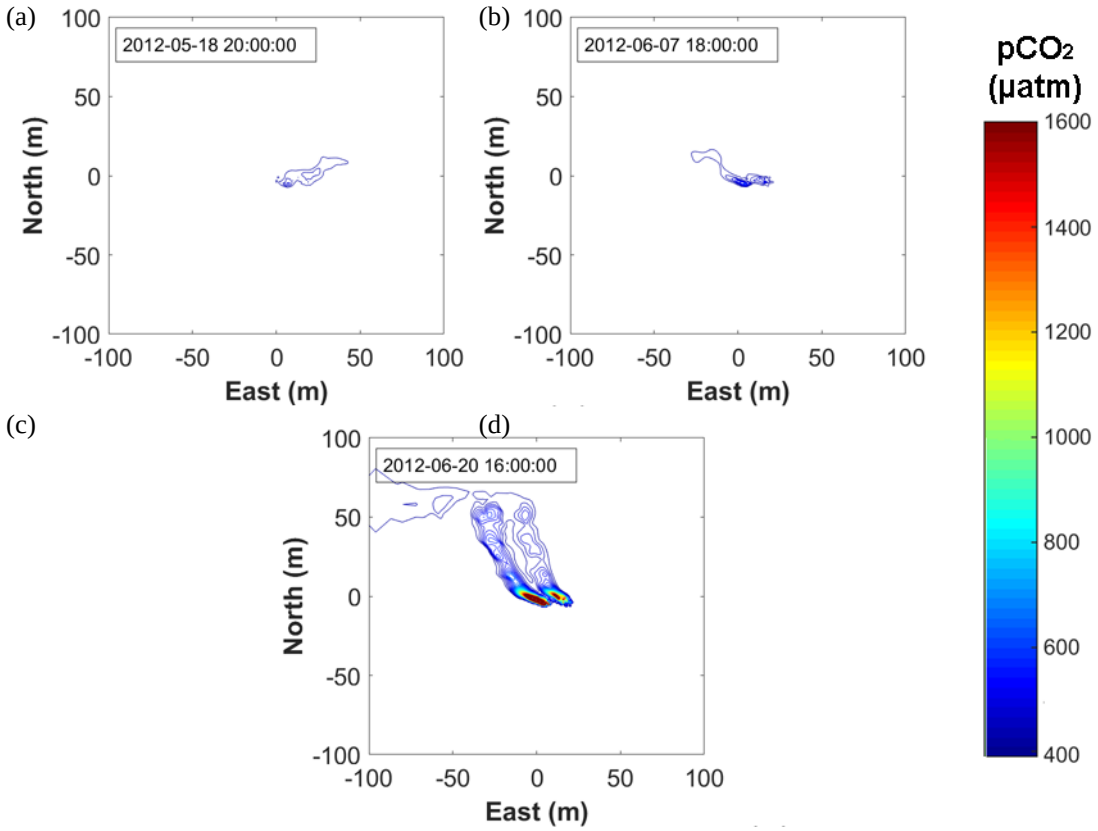

Figure 7. The simulated dissolved carbon plumes along the seabed at various timestamps for the QICS experiment, with the pCO_2 shown by the contour map at steps of 25 µatm. a) The low injection rate (80 kg/day on 17/05/2012), top left; b) The middle injection rate (170 kg/day on 06/06/2012), top right; c) The top injection rate (208 kg/day on 21/06/2012) bottom.

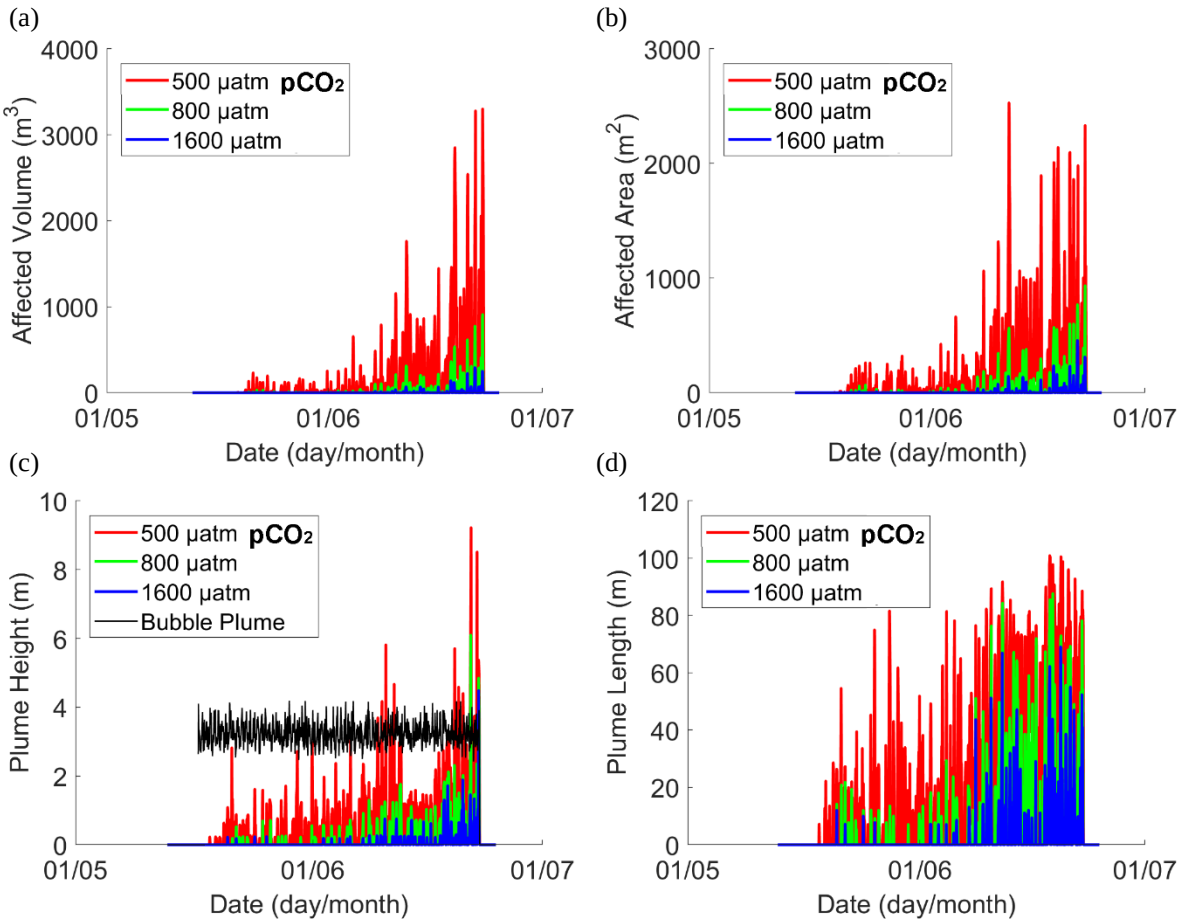

Figure 8. Analysis of the impact regions from the simulations of the QICS experiment for each pCO_2 threshold of 500 µatm (red), 800 µatm (green) and 1600 µatm (blue) over the course of the experiment. a) The affected volume of the water column, top left; b) The affected area on the seabed, top right; c) The maximum impact height of each threshold, plotted with the bubble plume height (black) for comparison, bottom left; d) The maximum impact length of the plume, bottom right.

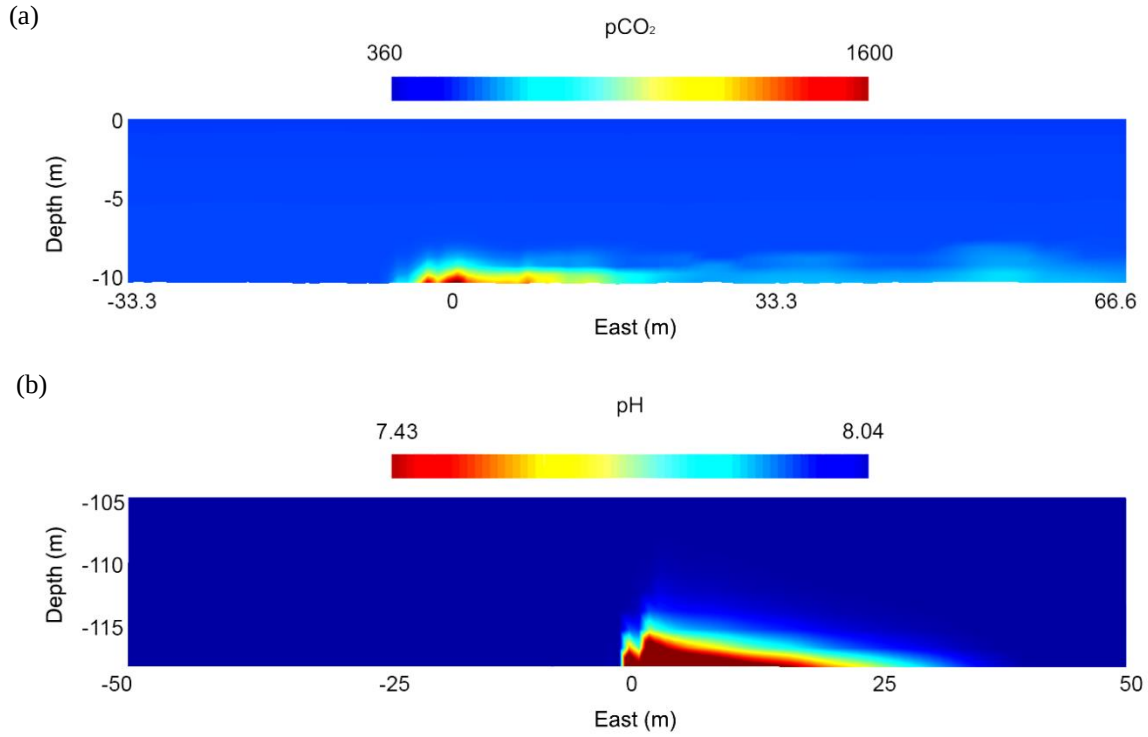

Figure 9. A snapshot of the release experiment pCO_2 and pH changes in a cross-sectional plot to show the vertical and horizontal impact. a) The pCO_2 changes in the QICS experiment, top; b) The pH changes in the STEMM-CCS experiment, bottom.

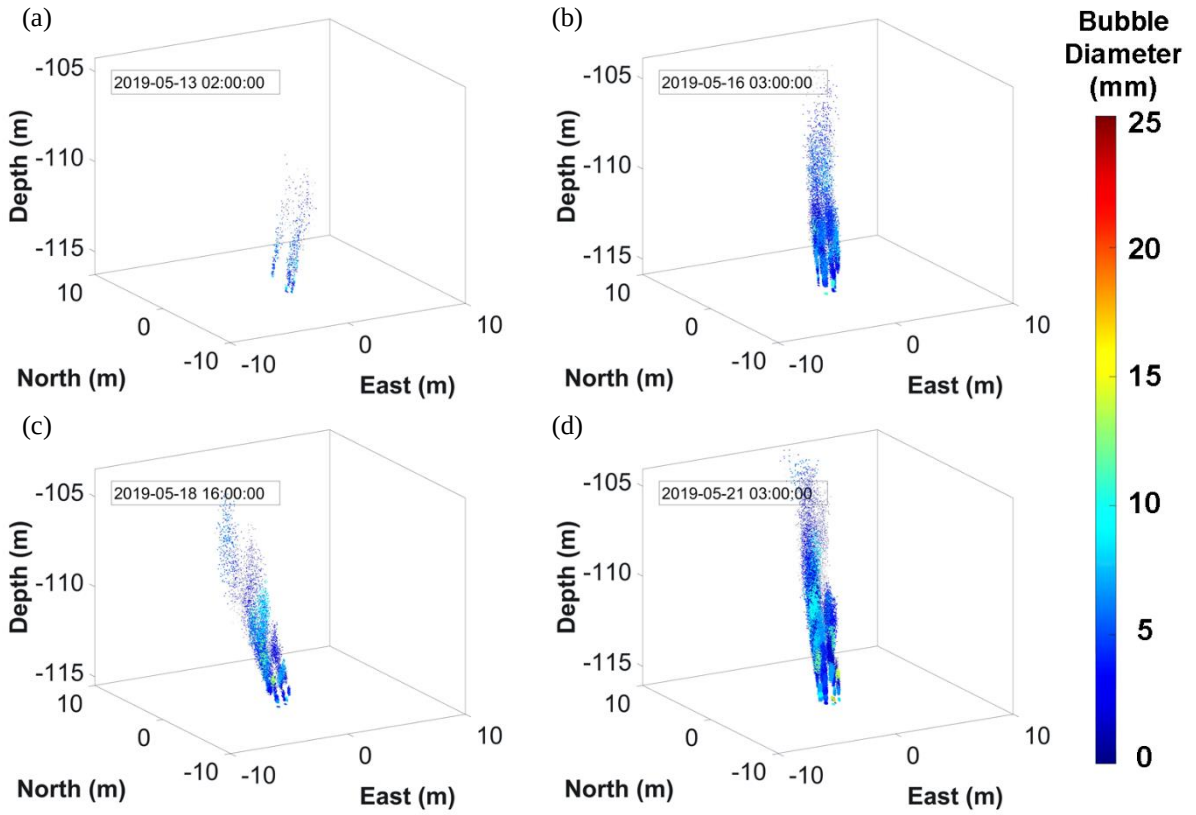

Figure 10. The bubble streams at various timestamps for the STEMM-CCS experiment for the PLUME model, with the bubble diameter (mm) shown by both the colour map and the size of the marker. a) Low injection rate (6 kg/day on 13/05/2019), top left; b) Increased injection rate (30 kg/day on 16/05/2019), top right; c) Middle injection rate (88 kg/day on 18/05/2019), bottom left; and d) Top injection rate (147 kg/day on 21/05/2019) bottom right.

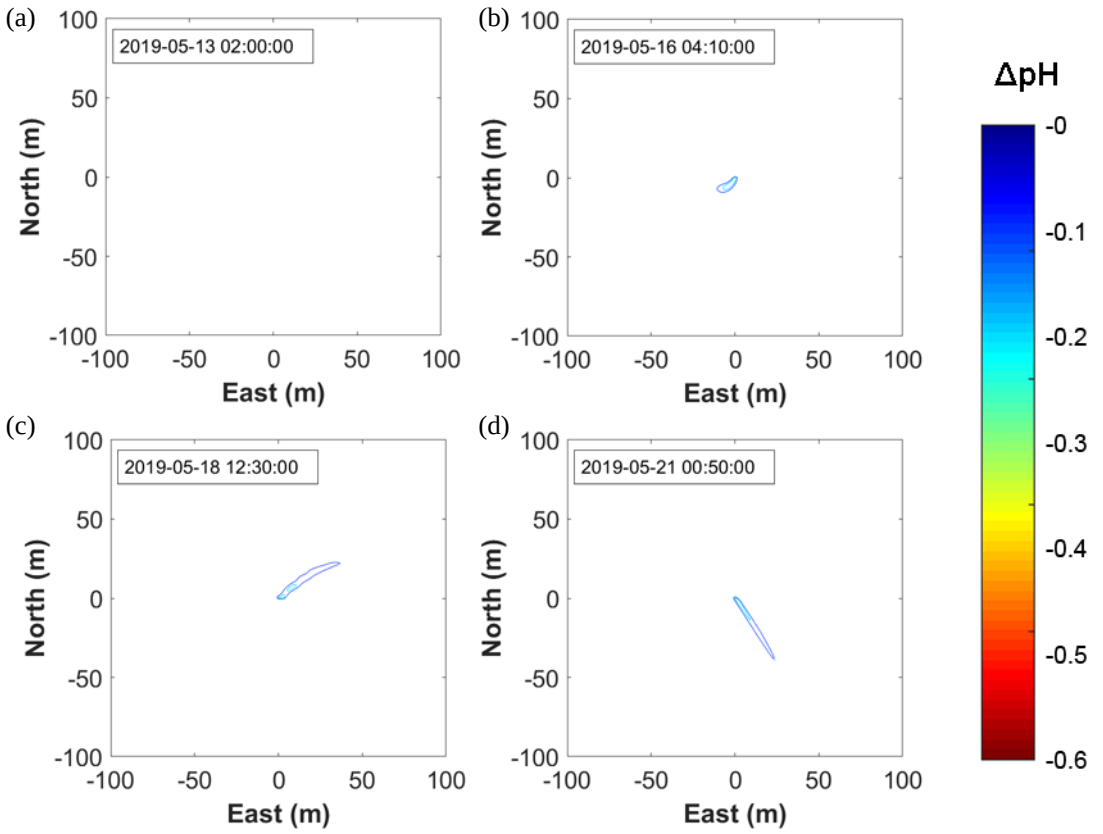

Figure 11. The dissolved carbon plumes developed along the seabed at various timestamps for the STEMM-CCS experiment from the simulations, with the changes in pH shown by the contour map at steps of 0.1 units. a) Low injection rate (6 kg/day on 13/05/2019), top left; b) Increased injection rate (30 kg/day on 16/05/2019), top right; c) Middle injection rate (88 kg/day on 18/05/2019), bottom left; and d) Top injection rate (147 kg/day on 21/05/2019) bottom right.

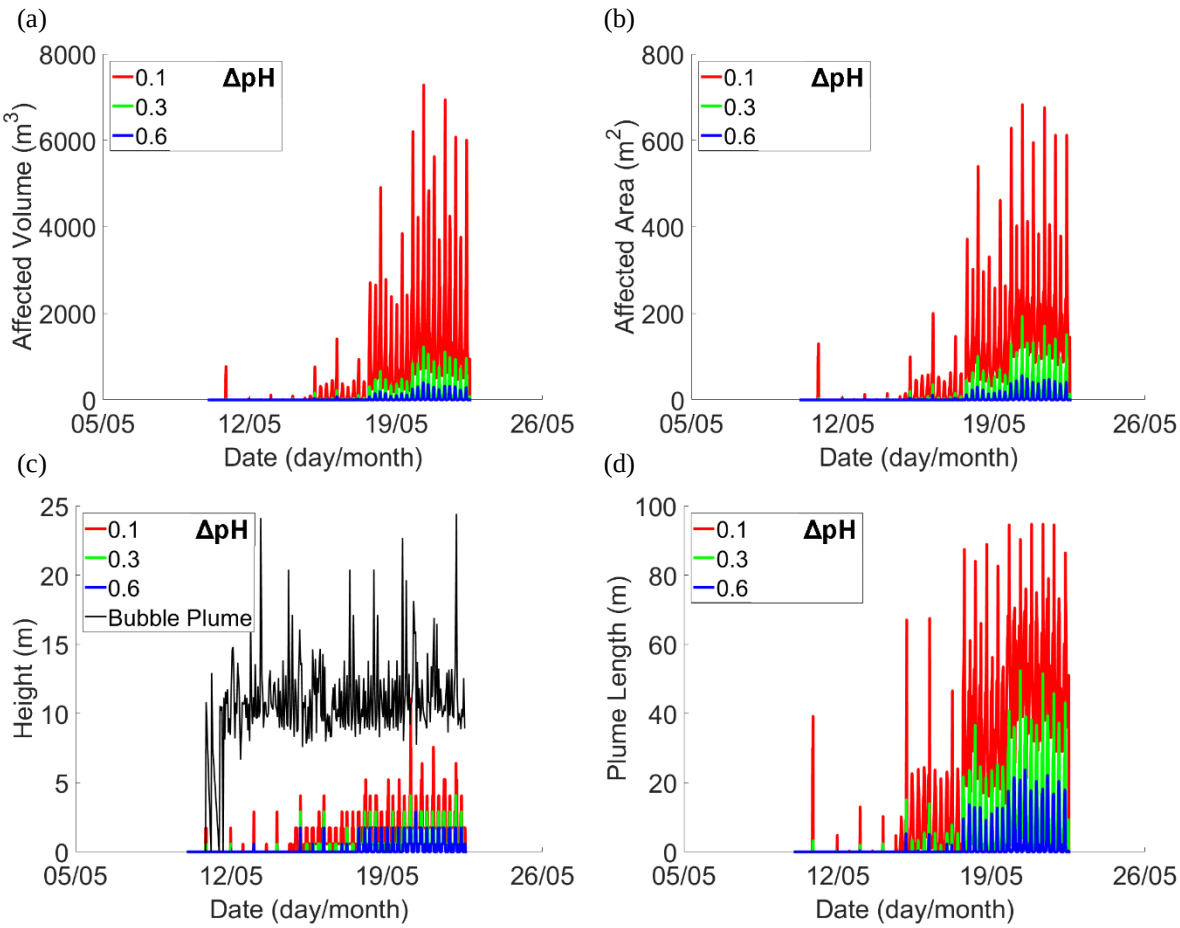

Figure 12. Analysis of the impact region from the simulations of the STEMM-CCS experiment for each pH reduction of 0.01 (red), 0.05 (green), 0.1 (blue) and 0.2 (magenta) over the course of the experiment. a) The affected volume of the water column, top left; b) The affected area on the seabed, top right; c) The maximum impact height of each threshold, plotted with the bubble plume height (black) for comparison, bottom left; d) The maximum impact length of the plume, bottom right.

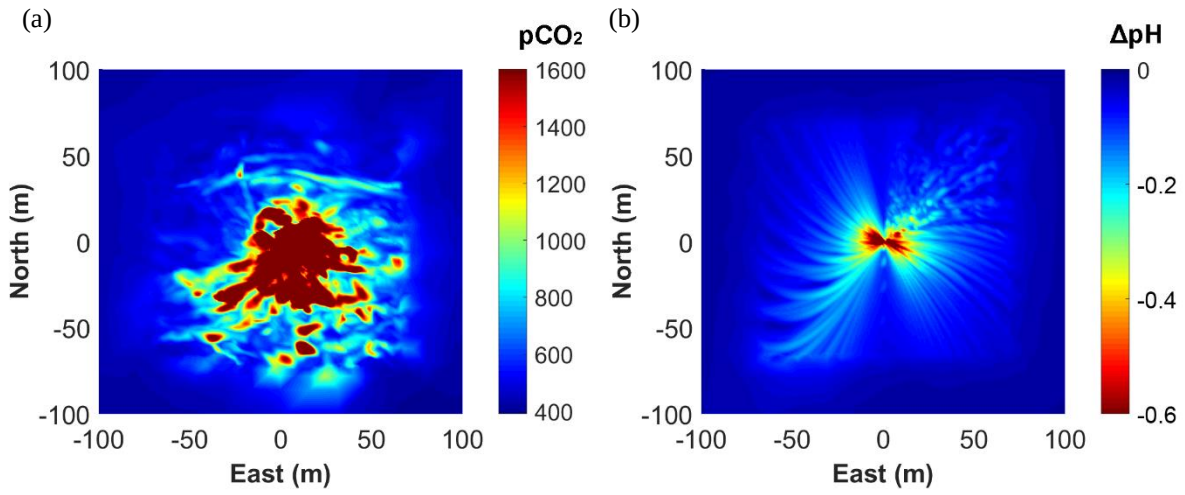

Figure 13. The impact regions over the course of the experiment from the simulations. a) The QICS experiment, with the pCO_2 shown by the colour map from hourly outputs, left; b) The STEMM-CCS experiment, with the pH shown by the colour map from 10 minute outputs, right.